AD NUMBER

ADB013636

LIMITATION CHANGES

TO:

Approved for public release; distribution is unlimited.

FROM:

Distribution authorized to U.S. Gov't. agencies only; Test and Evaluation; JUN 1976. Other requests shall be referred to Air Force Weapons Laboratory, DED, Kirtland AFB, NM 87117.

AUTHORITY

afwl ltr, 29 apr 1985

AD B013636

AUTHORITY: AFWL ltr, 29 Apr 85

AFWL-TR-76-16

AFWL-TR-
76-16

PROGRAMMABLE ACCELEROMETER CONDITIONER INTEGRATOR

June 1976

Final Report

Prepared for
Director
DEFENSE NUCLEAR AGENCY
Washington, DC 20305

AIR FORCE WEAPONS LABORATORY
Air Force Systems Command
Kirtland Air Force Base, NM 87117

This final report was prepared by the Air Force Weapons Laboratory, Kirtland Air Force Base, under Job Order WDNS0315. Captain David J. Ray (DED) was the Laboratory Project Officer-in-Charge.

This technical report has been reviewed and is approved for publication.

David J. Ray

DAVID J. RAY
Captain, USAF
Project Officer

FOR THE COMMANDER

James M. Warren

JAMES M. WARREN
Lt Colonel, USAF
Acting Chief, Developmental Branch

Frank J. Leech

FRANK J. LEECH
Lt Colonel, USAF
Chief, Civil Engineering Research Division

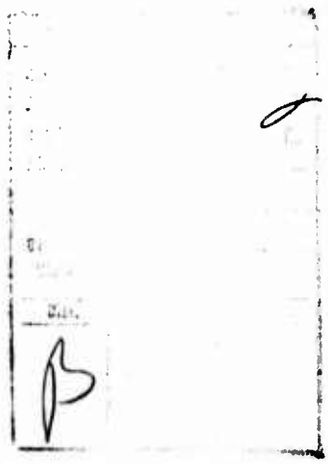

UNCLASSIFIED

SECURITY CLASSIFICATION OF THIS PAGE *(When Data Entered)*

REPORT DOCUMENTATION PAGE

READ INSTRUCTIONS BEFORE COMPLETING FORM

1. REPORT NUMBER: AFWL-TR-76-16	2. GOVT ACCESSION NO.
3. RECIPIENT'S CATALOG NUMBER	
4. TITLE *(and Subtitle)*: PROGRAMMABLE ACCELEROMETER CONDITIONER INTEGRATOR	5. TYPE OF REPORT & PERIOD COVERED: Final Report
6. PERFORMING ORG. REPORT NUMBER	
7. AUTHOR(s): 70 p.	8. CONTRACT OR GRANT NUMBER(s): F29650-76-C-0259
9. PERFORMING ORGANIZATION NAME AND ADDRESS: Air Force Weapons Laboratory (DED) Kirtland Air Force Base, New Mexico 87117	10. PROGRAM ELEMENT, PROJECT, TASK AREA & WORK UNIT NUMBERS: 62710H WDNS0315
11. CONTROLLING OFFICE NAME AND ADDRESS: Director Defense Nuclear Agency Washington, DC 20305	12. REPORT DATE: June 1976
	13. NUMBER OF PAGES: 70
14. MONITORING AGENCY NAME & ADDRESS *(if different from Controlling Office)*: Air Force Weapons Laboratory Kirtland Air Force Base, NM 87117	15. SECURITY CLASS. *(of this report)*: UNCLASSIFIED
	15a. DECLASSIFICATION/DOWNGRADING SCHEDULE

16. DISTRIBUTION STATEMENT *(of this Report)*

Distribution limited to US Government agencies only because of test and evaluation of military systems (Jun 76). Other requests for this document must be referred to AFWL (DED), Kirtland Air Force Base, New Mexico 87117.

17. DISTRIBUTION STATEMENT *(of the abstract entered in Block 20, if different from Report)*

18. SUPPLEMENTARY NOTES

19. KEY WORDS *(Continue on reverse side if necessary and identify by block number)*

Velocity Measurements
Integrator
Accelerometer Integrator
Signal Conditioner

20. ABSTRACT *(Continue on reverse side if necessary and identify by block number)*

Ground motion studies rely heavily on the Sandia DX velocity transducer. This report describes an analog circuit which may be used with a piezoresistive accelerometer to produce velocity data. The circuit may also be used to amplify and calibrate accelerometer outputs. It is programmable in that microswitches are used to change the gain and the low frequency roll-off point. The integrator is DC coupled, but it does not saturate with DC inputs. The results of laboratory tests and field test comparisons are described. It is concluded that

DD FORM 1 JAN 73 1473 EDITION OF 1 NOV 65 IS OBSOLETE

UNCLASSIFIED

SECURITY CLASSIFICATION OF THIS PAGE *(When Data Entered)*

013150 LB

20. ABSTRACT (Continued)

any integration schemes for producing velocity from acceleration data should be applied after the acceleration has been recorded and the final signal-to-noise ratio established. An improved routine for processing acceleration data is suggested.

CONTENTS

ILLUSTRATIONS

ILLUSTRATIONS (Continued)

TABLES

SECTION I

INTRODUCTION

Ground motion from high explosive tests may be described by the displacement, velocity or acceleration time history. Given the known boundary conditions (zero initial and terminal conditions for the velocity and all higher derivatives) along with any one of the time histories, the ground motion description is in theory complete, since the initial displacement is surveyed before the test. In practice, obtaining one time history from the other is complicated by the nonlinearities and noise introduced in the measurement process. For this reason, on high explosive tests, separate measurements of acceleration and velocity are ordinarily made using different types of transducers. The result is increased installation time and equipment for the instrumentation with a consequent increase in costs. Additionally, available accelerometers show less dependence on temperature and cross axis forces, along with fewer other nonlinear qualities than do currently available velocity transducers.

This report describes a method of obtaining velocity data from acceleration outputs. The approach used is one of simulating the transfer function of a currently used velocity gage by use of an accelerometer and an approximate second order integrator.

SECTION II

THE VELOCITY TRANSDUCER (DX)

The velocity transducer in common use today is the Sandia Laboratory's Model DX velocity gage. It is a redesign of an earlier gage developed by the Stanford Research Institute and is presently being commercially manufactured by Sparton Southwest, Inc., and Bell & Howell, Inc. The transducer consists of a pendulum in a viscous fluid with a carrier-excited variable reluctance sensing element which is, in turn, externally connected to an AC bridge circuit.

The differential equation of the velocity gage (ref. 1) when the case is subjected to a force in the direction U is

$$\ddot{\Theta} + 2h\omega_n\dot{\Theta} + \omega_n^2 \sin\Theta = \frac{\omega_n^2}{g}\dot{U}\sin(\phi - \Theta) \qquad (1)$$

Here the variables are

- Θ = pendulum angle
- h = damping factor
- ω_n = natural frequency
- g = acceleration due to gravity
- U = case velocity
- ϕ = angle between U and force of gravity

By linearizing about small pendulum angles and assuming perpendicular (horizontal) excitation, equation (1) becomes

$$\ddot{\Theta} + 2h\omega_n\dot{\Theta} + \omega_n^2\Theta = \frac{\omega_n^2}{g}\dot{U} \qquad (2)$$

The transfer function (in the complex frequency domain) may now be written as

$$H(s) = \frac{\Theta(s)}{U(s)} = \frac{\omega_n^2}{g}\,\frac{s}{s^2 + 2h\omega_n s + \omega_n^2} \qquad (3)$$

---

1. Schultz, George, "Mathematical Model and Closed Form Response Function for the Pendulous Type Velocity Transducer Subjected to Cross-Axis Inputs," Symposium on Advancement in Instrumentation for Civil Engineering Application, AFWL-TR-73-186, pp. 83-94, October 1973.

Since the steady state voltage of the system is presumed to be proportional to Θ, we may make the $s = j\omega$ substitution and observe that the magnitude of $V(j\omega)$ is constant with respect to the frequency of the velocity input only over the range where the $2h\omega_n$ term predominates in the transfer function. This range may be extended by increasing h. Figures 1a and 1b give the magnitude and phase character of the gage.

In the MIDDLE GUST series of tests (ref. 2), several velocity gages containing 500, 1000, and 3000 centistoke viscosity damping fluid were subjected to a step velocity input. For low frequency accelerations, the tests supported the model described by equation (2). However, the additional information of figure 2 from the same tests shows that the damping is a nonlinear function of the pendulum angular velocity. Substantial variations from the linear case occur at higher accelerations encountered using the sled track where the frequency content of the acceleration is higher. In figure 2, the retardation R is defined as

$$R = a - \ddot{\Theta} - \omega_n{}^2\Theta \tag{4}$$

where the input acceleration a is defined as

$$a = \omega_n{}^2 \dot{U}/g \tag{5}$$

Since the damping changes with acceleration level and frequency, the frequency response of the gage also changes.

The same series of MIDDLE GUST evaluation tests also showed a significant change in the damping factor for a change in temperature of the damping fluid. The change was found to be

$$h = Ae^{-PT} \tag{6}$$

where A is an amplitude constant, P is a constant, and T is the fluid temperature.

The curve shown in figure 3 is a best fit of the empirical data taken, again, from the MIDDLE GUST tests. It shows a temperature correction factor K in

---

2. Bunker, R., MIDDLE GUST Instrumentation Evaluation, AFWL-TR-72-238, December 1972.

terms of test, T_c, and ambient, T_a, temperatures. This correction factor must be applied to the velocity amplitude of the gage output. Consequently, it becomes apparent that small temperature variations can make significant errors in the amplitude of the velocity measurements.

The work of Schultz & Sonnenberg (refs. 1 and 3) shows that if the acceleration imparted to the velocity gage is not along the sensitive axis of the gage, the pendulum displacement and, consequently, the gage output are functions not only of the force $\dot{U} \sin \Theta$ along the sensitive axis of the gage but are also influenced by the force $\dot{U} \cos \Theta$ at right angles to that axis.

The deficiencies shown for the DX velocity gage originate in the mechanical fluid damped construction which causes anomalies and nonlinearities. Consequently, this device is currently undergoing severe analysis and has started considerable debate by experimenters in the ground motion community. From these discussions (ref. 4), the development of an electronically integrating accelerometer system was motivated. The current trend in this area* is that of using either a piezoresistive or piezoelectric accelerometer and various types of electronic integrating schemes to produce a voltage proportional to the velocity experienced by the accelerometer case. Only the piezoresistive type is treated here; the piezoelectric type may be analyzed in a similar manner. The properties of the piezoresistive accelerometer are well known, and available industry standards indicate that they possess advantages and superior performance over fluid damped pendulum gages (ref. 5).

---

*The following organizations are known to be or have been working on such approaches: Air Force Weapons Laboratory, Systems Science and Software, Bell & Howell, and USAF Academy Department of Electrical Engineering.

3. Schultz and Sonnenburg, Response Properties of an Orthogonal System of Pendulum-Type Velocity Gages, AFWL-TR-73-31, June 1973.

4. Symposium on Advancement in Instrumentation for Civil Engineering Applications, AFWL-TR-73-186, pp. 255-262, October 1973.

5. Bouche, R. R., "A Practical Application of Accelerometer Calibrations," The Shock and Vibration Bulletin, Naval Research Laboratory, Washington, D.C., December 1970.

SECTION III

ACCELERATION MEASUREMENTS

The piezoresistive accelerometer may be modeled as in figure 4. This is a typical second order spring, mass and dashpot system in which the mass in the model is connected to the sense arm of a potentiometer mounted to the case and which, in turn, is activated by a voltage source. In practice, a strain gage bridge is used. It is easily shown that if the case experiences an acceleration A, the output voltage in LaPlace notation is

$$V(s) = \frac{CA(s)}{s^2 + 2h\omega_n s + \omega_n^2} \tag{7}$$

where C is a constant determined by the excitation voltage. The choice for h now would be one resulting in a damping factor near the critically damped point. We would also choose the mass and damping to make ω_n as large as possible. A plot of voltage magnitude versus the acceleration frequency results in figure 5. For the piezoresistive accelerometer, a comparison of the voltage output with the case velocity gives the following transfer function and the spectra of figures 6a and 6b.

$$\frac{V(s)}{U(s)} = C \frac{s}{s^2 + 2h\omega_n s + \omega_n^2} \tag{8}$$

SECTION IV
INTEGRATION

1. TRUE INTEGRATION

Currently, computer integration using standard routines is done on acceleration data. The results, in general, have been unacceptable to many analysts using ground motion data. The reason for this stems from the integration of offset and low frequency hysteresis components in accelerometer outputs. This typically results in finite terminal velocities or in the presence of ramp functions in the velocity data. Both are contrary to the known boundary conditions of the experiment.

Offset voltages in the accelerometer are impossible to eliminate completely and must be considered as false signals which will be integrated with the true acceleration signal. The inevitable result is saturation of some portion of the data acquisition or reduction system. Various schemes are under development and test for establishing zero initial conditions in the integrating device just prior to the receipt of transient signals along with careful attention to reducing the accelerometer offset to the minimum possible value (refs. 6 and 7). This approach warrants investigation; however, a careful examination of the pendulum velocity gage presents the possibility of using an electrically equivalent concept.

2. APPROXIMATE INTEGRATION

The pendulum velocity gage does not give a true or perfect integration of the acceleration experienced by its case over all frequencies. This is obvious from figure 1. Of particular interest is the frequency range below the $\omega_n(h - \sqrt{h^2 - 1})$ point. Signals below this frequency are attenuated and therefore, cannot cause saturation unless they are extremely large. It is in this range that any offset or long period hysteresis signals would appear. An

---

6. Bunker, R. B., "Velocity Data Acquisition System," Symposium on Advancement in Instrumentation for Civil Engineering Applications, AFWL-TR-73-186, pg. 193, October 1973.
7. Gaffney, E. S., et al., ESSEX I-Phase 2-Code Verification Instrumentation-Stress and Velocity, Systems Science and Software, Report SSS-R-75-2465, La Jolla, California, October 1974.

electrical simulation of this type of transfer function would also have the properties of nonsaturation due to offsets and attenuation of low frequency hysteresis signals.

What we require is a device to integrate (as accurately as possible) all frequencies above a given point and attenuate (as much as possible) all frequencies below that point. For the velocity gage, this point is $\omega_n (h - \sqrt{h^2 - 1})$ in figure 1.

If the circuit with the following transfer function

$$H(s) = \frac{s}{s^2 + 2\omega_o s + \omega_o^2} \tag{9}$$

is cascaded with the accelerometer (where ω_o is the natural frequency of the circuit) the result is a fourth order approximation of the pendulum gage; that is

$$V(s) = C \frac{s^2 U(s)}{(s^2 + 2h\omega_n s + \omega_n^2)(s^2 + 2\omega_o s + \omega_o^2)} \tag{10}$$

where we choose $\omega_o << \omega_n$. This choice of constants is not unreasonable since the design of the accelerometer has already made ω_n very large.

If we now examine equation (10) over various ranges of s, the similarity between it and equation (3) becomes clear. Equation (10) can be approximated by

$$V(s) \approx C \frac{s^2 U(s)}{\omega_n^2 \omega_o^2} \approx 0$$

for

$$s << \omega_o$$

and reasonable values of U. Further

$$V(s) \approx C \frac{U(s)}{2h\omega_n \omega_o}$$

for

$$\omega_o << s << \omega_n$$

which is the desired relationship for a velocity system.

And, finally,

$$V(s) \approx C \frac{U(s)}{s^2} \approx 0$$

for $s >> \omega_n$

The magnitude and phase of V in equation (10) are plotted in figures 7a and 7b. It is interesting to compare figure 7 with figure 1. In figure 7, ω_n is the upper limit of the accelerometer response and ω_o is determined by equation (9). The only difference between the two devices is the roll-off rate above ω_n and below ω_o. The rate is now 12 dB per octave instead of 6 dB per octave in the case of the pendulum gage. Phase distortion is most pronounced near the magnitude break points.

Equation (9) is, of course, recognized as the transfer function for a second order bandpass filter with a Q of one-half. There presently exists in circuit theory literature a myriad of active circuits which can perform this function, and the reader is referred to reference 8 as one possible source of such circuits.

The center frequency of the filter is placed such that the frequencies to be integrated are above the center frequency while all undesirable long period drift frequencies are considerably below center frequency. Figure 8 gives a comparison of the frequency and phase response plots of a true integrator and an approximate integrator for the integration of frequencies above 10 radians per second.

3. APPROXIMATE INTEGRATOR CIRCUIT DESCRIPTION

The circuit proposed in this report to give the transfer function of equation (9) is shown in figure 9. Equation (11) gives the transfer function in terms of the circuit parameters. The U.S. Government has applied for a patent on this circuit.

$$\frac{V_o}{V_i} = \frac{\frac{1}{R_1C_1}\, s}{s^2 + \left(\frac{1}{R_dC_1} + \frac{1}{R_2C_2}\right) s + \frac{1}{R_2C_2}\left(\frac{1}{R_dC_1} + \frac{1}{R_1C_1}\right)} \qquad (11)$$

8. Budak, Passive and Active Networks, Analysis and Synthesis, Houghton Mifflin Company, Boston, Massachusetts, 1974.

One choice of normalized values which gives a normalized frequency of 1 radian per second is

$$R_1 = 0.156\ \Omega$$

$$R_2 = 1\ \Omega$$

$$R_d = 0.277\ \Omega$$

$$C_1 = 2\ \text{fd}$$

$$C_2 = 5\ \text{fd}$$

This results in an approximate transfer function of

$$\frac{V_o}{V_i} = \frac{3.2s}{s^2 + 2s + 1}$$

SECTION V

THE VELOCITY SYSTEM

The remaining task is to interface the differential output piezoresistive bridge to the single ended input of the active integrator. In addition, it is desirable that the acceleration pulse be amplified. This interfacing and amplification can be accomplished by the insertion of a differential input instrumentation amplifier (such as the Analog Devices AD520J) between the accelerometer and the integrator.

The resulting velocity system is shown in figure 10. The gain of the instrumentation amplifier must be set at a value which will not result in saturation of the instrumentation amplifier itself or of the integrator. An approximate knowledge of the acceleration pulse is required since the integrator may be saturated by either a high amplitude, short duration pulse or a low amplitude, long duration pulse.

In typical applications, the system is calibrated by shunting a precision resistor across one arm of the accelerometer. The resulting velocity output may then be calibrated in appropriate engineering units. If calibration is to take place shortly (seconds) before an actual signal input to the integrator, the settling time of the integrator may be too long. In this case, the calibration resistor should shunt first one side of the bridge and then the other for equal lengths of time. The integrator will thus be driven back to near zero in preparation for the event to be measured.

SECTION VI

PROGRAMMABLE ACCELEROMETER CONDITIONER INTEGRATOR (PACI) SYSTEM AND CIRCUIT

1. THE SYSTEM

The PACI system is essentially a near hole signal conditioner with an optional integrating circuit. It contains integrated circuit timers and micro-relays for calibration. This calibration circuit is independent of the amplifier/integrator circuit. Figure 11 is a block diagram of PACI. The unit requires ± 12 to ±15 volts power for all circuits except the calibrate circuit which requires +5 volts power. A schematic of the PACI circuit is shown in figure 12. The parts list for the PACI circuit is contained in the appendix.

2. AD520J INSTRUMENTATION AMPLIFIER

This part of the circuit is essentially the same as other standard signal conditioners using the AD520J. The gain is programmed using three micro rocker switches. A potentiometer is included for offset adjustment.

3. NONSATURATING INTEGRATOR

The AD520J is automatically fed into a nonsaturating integrator consisting of two UA 741 operational amplifiers. Amplifier U2 is an integrator. The output of U2 is then integrated by U3 and this displacement signal is returned to the negative input (Pin 3) of U2. The time constant (low frequency roll-off point) of the integrator is determined by R16, R17, and R18 in combination with C12, 13, 14, 15, 16 and 17. By closing S8 through S11 in the proper combination, an appropriate time constant of 0.1, 1, and 10 Hz may be chosen. The following table gives the switch combination for a corresponding time constant.

TIME CONSTANT	S8	S9	S10	S11
0.1	0	0	0	0
1	0	CL	0	CL
10	CL	CL	CL	CL

The integrator has an offset adjust through R19. However, U4 should have its offset balanced out before balance is attempted on the integrator. Switch S1 is

used to send the velocity signal to U1, the line driver. Switch S2 is used to send displacement data to U1. Either S1 or S2 but not both may be closed.

4. LINE DRIVER

U1 provides gain for the velocity or displacement outputs. The gain is programmable by S3 and S4. The gain of U1 is calculated by

$$\frac{R_f}{R_{in}}$$

where R_f is the equivalent series resistance of R22, 23, and 24 and whatever combination of S3 and S4 is chosen. R_{in} is either R20 or R21 depending on whether S1 is closed or S2 is closed. S1 closed and S2 closed is an invalid combination.

5. CALIBRATE CIRCUIT

Two NE555 timers are the basic components of this portion of the circuit. Pin 2 is the input trigger. Only the falling edge of a pulse will start the NE555 output pulse which is taken from Pin 3. Q1 inverts the leading edge of the incoming trigger. The resulting inversion starts U6 in its monostable function. The trailing edge of the input trigger is applied directly to U5. Figure 13 gives the time sequence.

Q2 and Q3 are driving transistors for K1 and K2. R4 and R5 adjust the length of the output pulse for U6 and U7, respectively. Rcal is the calibration resistor for the bridge. Bridge balance is achieved by RBal and R11.

6. PACI PROGRAM INSTRUCTIONS

The PACI System contains two amplifiers and a circuit for either integration or double integration. To use this system, one must know what gains are needed at each stage to (1) prevent saturation of any stage and (2) provide a signal output level which is as high above the noise level as possible. In some cases, the follow-on multiplex or recording system may dictate a reduced output level.

The PACI output voltage (V_o) may take any of the following three forms.

$$V_o = G_1 (V_1 - V_2) \qquad (1)$$

$$V_o = G_1G_2G_3 \int_0^t (V_1 - V_2)dt \qquad (2)$$

$$V_o = G_1G_2G_3 \int_0^\tau \int_0^t (V_1 - V_2)dt\, d\tau \qquad (3)$$

Here, G_1, G_2, and G_3 are gain constants determined by the positions of the micro rocker switches labeled S3 through S11. Switches S1 and S2 determine whether the output voltages take form (2) or (3) above. Output voltage form (1) is a separate output pin on the printed circuit card and is always available.

Gain G_1 is the gain of the AD520J instrumentation amplifier and is determined by switches S5, S6, and S7. Gain G_3 is determined by switches S1, S2, S3, and S4. It is used for single integrated outputs when S1 is closed and S2 is open. A different Gain G_3 is used for double integrated signals when S1 is open and S2 is closed.

Gain G_2 is associated with the integrator. This gain is a by-product of the desired low frequency response. Ordinarily, it is not under the control of the programmer since the required low frequency response dictates the value of G_2.

Actual values of the gain constants and the required switch positions are summarized in tables 1 through 4 as are the PACI functions. Here, a 0 means open and a 1 means closed. An X means no effect on that parameter.

Table 1

REQUIRED SWITCH POSITIONS

Function	Output Pin	S1	S2
Amplifier	E	X	X
Integrator	B	1	0
Double Integrator	B	0	1

Note: S1 and S2 closed is an invalid combination.

Table 2

G_1 GAIN VALUES

G_1	S5	S6	S7
5.9	0	0	0
6.7	0	0	1
8.2	0	1	0
9.8	0	1	1
11.5	1	0	0
14.9	1	0	1
25.0	1	1	0
50.0	1	1	1

Table 3

G_3 GAIN VALUES

G_3	S1	S2	S3	S4	Function
0	0	0	X	X	
100	0	1	0	0	
61	0	1	0	1	Displacement
49	0	1	1	0	
10	0	1	1	1	
19.6	1	0	0	0	
12.0	1	0	0	1	
9.6	1	0	1	0	Velocity
1.9	1	0	1	1	

Note: S1 and S2 closed is an invalid combination.

Table 4

G_2 GAIN VALUES

G_2	S8	S9	S10	S11	Low Frequency Cut-Off
139	0	0	0	0	10 Hz
12.6	0	1	0	1	1 Hz
1.43	1	1	1	1	0.1 Hz

7. SELECTION OF PARAMETERS

a. Acceleration Only

Here, the output is taken on Pin E as indicated by table 1. A suitable gain is chosen by dividing the desired output by the predicted gage signal level and then choosing the next lowest value for G_1 in table 2.

b. Velocity

The program for velocity is complicated by the fact that both the predicted acceleration and the predicted velocity are needed. The predicted acceleration a in ft/sec^2 is integrated as if it were a square pulse (which it really is not) in which case, the following holds

$$T = \frac{V}{a}$$

where V is the velocity in ft/sec and T is the duration of a. Once T is known, multiply the predicted gage voltage level for a by T, G_1 and G_2 to get the velocity voltage out of the integrator. Gain G_3 is then selected as needed. An example follows.

A 10,000 G accelerometer is predicted to experience 4,000 G acceleration and a peak velocity of 80 ft/sec. Its voltage output at the predicted acceleration level will be 100 mV. The first amplifier Gain G_1 was previously selected to be 14.9.

1. First find a value for T presuming a pulse input of 4,000 G or 128,800 ft/sec^2.

$$T = \frac{80}{128,800} = 0.62 \text{ msec}$$

2. Now find the velocity voltage out of the integrator (presume we have selected the 1 sec time constant range with a resulting $G_2 = 12.6$).

$$V_o = 100 \times 10^{-3} \text{ sec} \times 6.2 \times 10^{-4} \times 14.9 \times 12.6$$

$$= 0.0117 \text{ volt for a velocity of 80 ft/sec.}$$

3. Since this is rather low, use Gain G_3 to increase the level by 19.6. The resultant velocity voltage out of Pin B is therefore, expected to be 0.229 V at 80 ft/sec.

4. To set the tape recorder band edge at twice the expected value, set upper and lower band edges at $\pm$ 0.458 volt.

A word about what value to use for G_2. The decision for switches S8 through S11 must be made by considering the frequency content of the expected velocity signal. For the DX velocity gage, this is done by selecting a particular oil. Generally, large explosions with measurements at greater distances require low frequency response and this means S8 through S11 closed resulting in G_2 = 1.43. The low frequency response goes down to 0.1 Hz. For small explosions and close-in measurements, one might choose S8 through S11 open resulting in a G_2 of 139 and the low frequency response now only goes down to 10 Hz. For S8 and S10 open, S9 and S11 closed, the low frequency response is 1 Hz and G_2 is 12.6. This is summarized in table 4.

c. Displacement

The displacement feature of the PACI system is useful only in very limited applications and has not yet been satisfactorily tested. Its use is not presently contemplated; therefore, it is not discussed here.

d. Calibration

Acceleration calibration is no different than presently-used systems. A calibration resistor is chosen and the resulting pulse-out has a level that is a known acceleration. The velocity calibration is a ramp function which is the integral of a known acceleration for a known time. By measuring the slope of the ramp, one can read the velocity at any point.

SECTION VII

LABORATORY TESTS

After assembly, the PACI circuit was tested in the AFWL/DEX laboratory. The circuits operated as designed. The results of the calibration circuit operation were detailed in an earlier report on the prototype version of PACI. That report was AFWL-TR-73-255, titled, "Development of a Pseudo Integrator for Improved Velocity Measurements."

Tests were made of the integrator frequency response. Figure 14 shows the responses for each of the three integrator time constants. The response for time constant 2 does not match the expected value because of a measurement reading error.

Figures 15 and 16 give the integrator output for time constant 1 when driven by a square wave of fundamental frequencies 2 and 5 hertz, respectively. The deviation from the desired straight line output, as shown in figure 17, is in the worst case, less than 10 percent.

SECTION VIII

FIELD TESTS

1. PRE MINE DUST

The first prototype version of PACI was field tested in July 1973 on the PRE MINE DUST tamped HE Event at the Nevada Test Site. The results of that test were included in reference 9. In that report, the acceleration signals were also recorded. These signals were computer integrated and the results compared to the PACI velocity signals.

2. ESSEX 6 MWS

a. Test Description and Measurements

In June of 1974, the finalized version of PACI (same as described in a previous section of this report) was fielded on the ESSEX I, PHASE II, 6 Meter Water Stemmed Event near Ft. Polk, Louisiana.

Each channel of the system fielded used a piezoresistive accelerometer which was then cascaded with PACI. The resultant fourth order system output was approximately 7 percent linear with respect to sensor case velocity over the following ranges.

Gage Acceleration Range	Frequency Response (7% Linear)
10 kG	0.5 Hz to 10 kHz
2.5 kG	0.5 Hz to 7 kHz
250 G*	0.5 Hz to 3 kHz

*G = Acceleration of Gravity

Here, the upper cut-off is determined by the accelerometer and the lower cut-off is determined by the PACI integrator. Above and below the cut-off frequencies, the response falls off at 12 dB per octave. Other recorder outputs from the electronics were amplified acceleration and displacement.

---

9. Bunker, R. B., et al., Development of a Pseudointegrator for Improved Velocity Measurements, AFWL-TR-73-255, pp. 25-38.

Each accelerometer was placed at shot depth (6 meters) and grouted. Gage cables were run through tubing to ground level and then in buried trenches to the electronics package placed in a protected box 300 feet from ground zero. Table 5 summarizes each gage distance and range. Table 6 gives the recorded electronics outputs and levels.

Table 5

SUMMARY OF GAGE DISTANCE AND RANGE

Gage #	Distance From GZ	Range of Gage	Cal Level	Prediction	Remarks
1	12 meters (39.4 ft)	10 kG	4.588 kG	5 kG	Failure of gage or cable at t+30 msec
2	24 meters (78.8 ft)	2.5 kG	1.820 kG	1.5 kG	Failure of gage or cable at t+403 msec
3	36 meters (118.1 ft)	2.5 kG	0.814 kG	0.6 kG	Failed before test
4	48 meters (157.5 ft)	250 G	0.190 kG	0.2 kG	Data arrival at t+23 msec

Table 6

RECORDED ELECTRONIC OUTPUTS AND LEVELS

Output #	Gage #	Type Output	Cal Level (volts)	100% Band edge	Remarks
1	1	Acceleration	2.8	10.8	
2	1	Velocity 1	4.5	11.5	1 Hz low freq. roll-off
3	1	Displacement	0.95	3.8	
4	1	Velocity 2	0.78	1.8	10 Hz low freq. roll-off
5	2	Acceleration	3.5	11.3	
6	2	Velocity 1	4.6	11.7	1 Hz low freq. roll-off
7	2	Displacement	1.4	5.6	
8	2	Velocity 2	1.0	3.0	10 Hz low freq. roll-off
9	4	Acceleration	7.2	11.7	
10	4	Velocity 1	10.0	11.2	1 Hz low freq. roll-off
11	4	Displacement	1.9	3.0	
12	4	Velocity 2	1.6	1.7	10 Hz low freq. roll-off

From the electronics package, the signals were routed through 10,000 feet of 20 pair cable to the Waterways Experimental Station Recording Van.

b. Results

Only Gages 1, 2, and 4 were functional at event time. Of these, Gage 4 gives the most acceptable data and, consequently, can be used to compute a shock wave speed of 6,500 feet (or 2,000 meters) per second. Using this value, data arrival times of 6 msec and 12 msec can be expected for Gage 1 and Gage 2, respectively.

GAGE 1 ACCELERATION. Figure 18 gives the amplified acceleration output of Gage 1. Considerable noise is encountered at t+0. One pulse occurs at t+5.3 msec and has a peak value of the expected 5,000 G level. This pulse may contain ground motion data. Either gage or cable failure occurs at t+30 msec.

GAGE 2 ACCELERATION. Figure 19 gives the amplified acceleration of Gage 2. The data pulse appears to occur at 11.2 msec. As ground acceleration information, this pulse is suspect since its positive acceleration is not matched by a corresponding deceleration. Gage or cable failure occurs at t+403 msec.

GAGE 4 ACCELERATION. Data arrival time appears to be at t+23.7 msec. The fourth negative peak appears to have driven the gage into resonance. Figure 20 also suggests more acceleration than deceleration which should result in a terminal nonzero velocity.

GAGE 1 VELOCITY. Figures 21 and 22 display the first and second velocity traces for Gage 1. The low data amplitudes and high noise levels combine to obfuscate any ground motion information.

GAGE 2 VELOCITY. Figures 23 and 24 display the first and second velocity outputs of Gage 2 and, again, the data are plagued by noise. However, enough velocity information is seen to confirm the suspicion that the accelerometer output contains all acceleration and no corresponding deceleration until possible cable breakage. This results in the terminal nonzero velocity.

GAGE 4 VELOCITY. Figure 25 displays the first velocity plot for Gage 4. The 14 track instrumentation tape presently on file at AFWL Data Reduction contains no information on that track assigned to ESSEX Gage 4, Velocity 2. Since these are data from an experimental system, it is most important to compare this information with that received from other measurement schemes at the same station.

DISPLACEMENT OUTPUTS - ALL GAGES. Excessive noise precludes the retrieval of displacement information.

c. ESSEX Comparison

The quality of data on the 12 and 24 meter distance channels was not good enough for comparison. The Army Waterways Experimental Station (WES) provided pendulum velocity gage data for comparison at the 48 meter station. Figure 26 is the WES comparison.

3. PRE MINE THROW IV, EVENT 6

The Air Force Weapons Laboratory fielded three add-on ground motion measurements on the PRE MINE THROW IV Event. The outputs from three piezoresistive accelerometers were run to the integrators and gage support circuitry which was placed in a protected position about 300 feet from the first gage. The calibration circuitry proved to be shock sensitive. From this protected position, the signals were routed via buried cables to the Physics International Instrumentation Van to be recorded. Table 7 summarizes the pertinent information for each channel.

Each accelerometer package was placed at a depth of 59 inches to correspond with other gages located by Physics International. Cables were buried at 24 inches and run to the Instrumentation Electronic Station at 320 feet on the N75°W reference radial. The PACI electronics was housed in a rack with a battery power supply and then placed in a four foot square plywood container. This was covered with a 2 inch x 6 inch x 4 foot lid and sandbagged.

Results. All gages functioned throughout calibration, the test event, and post calibration. From accelerometer Station A5A and A7A, the velocity of the ground shock averages to 6,545 feet per second.

The calibration of each gage was by means of the previously described microrelay located at the protected electronic integrator position. When the ground shock arrived at this position, it jolted the relays with sufficient force to cause several calibration closures in the later part of the data. The velocity data were especially affected by this.

The following figures give the result of each channel for 600 ms. In some cases, the spurious calibrations were removed by computer techniques.

Table 7

PRE MINE THROW IV PACI ADD-ON PLOTS

Figure	Station	Orientation	Measured Parameter	Computer Integrated Parameter
27	5	R	Acceleration	Velocity
28	5	R	Velocity	Displacement
29	5	V	Acceleration	Velocity offset removed
30	5	V	Velocity	Displacement
31	7	V	Acceleration	Velocity offset removed
32	7	V	Velocity	Displacement

STATION 5 RADIAL ACCELERATION. The radial accelerometer located at Station A5V, figure 27 (trace inverted), 125 feet from ground zero had a signal arrival time of 19.5 ms that was outward and reached a peak acceleration of 65 G at 20.5 ms, followed by an inward peak acceleration of 120 G occurring at 22 ms.

STATION 5 RADIAL VELOCITY. The peak outward velocity, figure 28 was approximately 4 fps occurring at 21.2 ms while the peak inward velocity of 1 fps was reached at 23.2 ms. Utilizing the arrival time of 19.5 ms, a propagation velocity of 6,410 fps was calculated. The record shows a trend toward zero terminal velocity. Although not shown, the noise level of Channel 1 was excellent until zero time indicating that some noise may have been induced electrically.

STATION 5 VERTICAL ACCELERATION. The accelerometer A5R, figure 29, located 125 feet from ground zero showed downward motion at 19.5 ms. Peak amplitude of 160 G was reached at 21.5 ms. A propagation velocity of 6,410 fps was calculated using the arrival time of 19.5 ms.

STATION 5 VERTICAL VELOCITY. The velocity peak of 11.2 fps, figure 30 (trace inverted), occurred at 23 ms and did not reach a zero terminal velocity at graph termination time. Although not shown, this record is extremely noise-free until zero time indicating possible induced electrical noise. Spurious calibration pulses occurred at 150, 230, and 290 ms.

STATION 7 VERTICAL ACCELERATION. The A7V vertical accelerometer, figure

31 (trace inverted), located 204 feet from ground zero had an initial signal time-of-arrival of 31.0 ms and a peak acceleration of 23 G at 32.6 ms. The largest peak acceleration of 50 G occurred at 36.5 ms. Utilizing the TOA of 31.0 ms, a velocity of 6,580 feet per second was calculated. Although now shown, the noise level of this channel was excellent until zero time occurred indicating that some noise may have been introduced electrically.

STATION 7 VERTICAL VELOCITY. The peak velocity of 6.1 fps, figure 32 (trace inverted), occurred at 38.9 ms. The record does not show a zero terminal velocity. Although not shown, the noise levels were excellent until zero time indicating electrically induced noise may have occurred.

Comparison. Information pertinent to the Physics International measurements is included in Table 8.

Table 8

PRE MINE THROW IV, EVENT 6 MEASUREMENT DATA

Station No. PI No.	J-Box No.	Distance (ft)	Orientation	Gage & Amplifier No.	Gage Range Acc. or Vel.	Cal Level Acc. or Vel.	Predicted Acc. or Vel.	Cal Volts to Tape 0 to Peak	Tape Track No.	Cal Deviation	Bias On Signal
A5V / A5	3	125	V	AB55	250 G	190	154 G	5	10	80%	-2.63 V
V5V / A5	3	125	V	AB55	15.2 f/s	15.2	8 to 15 f/s	1.1	11	100%	0
A5R / A5	2	125	R	AB74	250 G	198	154 G	7.5	8	80%	0
V5R / A5	2	125	R	AB74	16.0 f/s	16.0	2 to 5 f/s	1.5	9	100%	0
A7V / A7	1	204	V	AB13	250 G	145	100 G	7.0	6	80%	0
V7V / A7	1	204	V	AB13	15.8 f/s	15.8	5 to 9.5 f/s	1.8	7	100%	0

The Physics International measurements utilized overdamped pendulum gages and Bell & Howell integrating accelerometers. Apparently, due to the lower frequency response of the pendulum gage, a significant difference in maximum particle velocity is shown. Physics International did not obtain any data at Station 7, so a comparison with AFWL data can only be made at Station 5. A data trace from a Bell & Howell integrating accelerometer from Station 5 is shown in figure 33. It shows an initial downward particle velocity of 11.25

feet per second followed by an upward velocity of 1.5 feet per second and a zero terminal velocity at 500 milliseconds. This may be compared with PACI results in figure 30 which indicate an initial downward velocity of 11 feet per second and an upward velocity of 1 foot per second. A pendulum gage located at this station measured an initial peak downward velocity of 8 feet per second followed by an upward peak of about 2 feet per second, as shown in figure 34. It would appear that at station 5 the pendulum velocity gage did not respond to the high short duration initial velocity peak that both of the integrating accelerometers recorded. A horizontal ground motion measurement for Station 5 from a Bell & Howell accelerometer is shown in figure 35. This record shows an outward velocity of 9 inches per second with a recovery of about 6 inches per second. This measurement may be compared with PACI results in figure 28 which show an outward velocity peak of 4 feet per second at 23 milliseconds with a sharp rebound of 1 ft/sec at about 25 ms. The remaining portions of both traces follow closely with peaks at 90, 170 and 230 ms. The following table compares these peak amplitudes.

	90 ms	170 ms	230 ms
Bell & Howell Amplitude	+1.9 ft/sec	-1 ft/sec	+1.2 ft/sec
AFWL Amplitude	+3.2 ft/sec	-1.5 ft/sec	+.9 ft/sec

Table 9. Station 7 Late Time Peak Amplitude Comparison

SECTION IX

CONCLUSIONS

The PACI concept was applied with analog circuits located in a protected position near the transducer. The advantage of recovering velocity data comes from its inherently lower frequency content when compared to acceleration data. It is assumed that the long line is frequency limited in the region of the acceleration data frequencies or that the multiplex system or recording method is also band limited. However, the placement of electronics at or near the transducer can also lower the driving point impedance of the line to a point where the frequency response of the cable is significantly higher than the acceleration data.

Unless the signature of the velocity is accurately known before the event, it is desirable to record acceleration data. This stems from the inherent noise floor in the data acquisition system. If the integration is performed before the noise is introduced, any inaccuracy in the prediction on the high side will result in unrecoverable velocity data on the high frequency side. The greater the inaccuracy, the greater will be the frequency loss as seen in the ESSEX data of this report. Integration after noise introduction, however, has no effect on the signal-to-noise ratio over the entire velocity spectrum provided reasonable care in signal reduction and integration is taken.

Using the low frequency roll-off method as applied in the PACI concept presumes a knowledge about the low frequency character of the velocity data, namely, that some lower bound exists on the velocity frequency content. The acceleration signal is integrated down to this point and all lower frequencies are attenuated. It is this attenuation of the presumed spurious low frequencies that brings the velocity trace back to zero. If the low frequencies are attenuated before the data are recorded, these frequencies may be lost. Consequently, if the roll-off point was incorrectly chosen, valuable data may be lost.

The arguments given above lead one to conclude that any integration schemes for producing velocity from acceleration data should be applied after the acceleration has been recorded and the final signal-to-noise ratio established. The use of the PACI low frequency roll-off concept may then be applied to the

recorded acceleration over and over. With each run, the low frequency roll-off point may be changed. At some point, the velocity trace will return to zero at the same time that the derivative of the acceleration reaches final zero. This would then be the limit of the accuracy of the concept. Since, as stated earlier, noise is a primary consideration, it would be advantageous to digitize the acceleration data to preserve its signal-to-noise ratio. At this point, a digital routine which duplicates the PACI concept would be preferable to PACI analog processing.

The PACI low frequency roll-off concept may be improved further with the use of digital routines. After one chooses the low frequency roll-off point, a multiple (6-8) pole digital high pass filter is programmed at the roll-off point. The result of this prefiltering may then be integrated using standard integration routines. The advantage here is a much steeper cut-off on the low frequency end.

In summation, the following conclusions were reached in the development of a Programmable Accelerometer Conditioner Integrator.

a. The integration of acceleration to derive velocity should be done after the signal is recorded in permanent storage.

b. Electronic amplifiers should be used at the accelerometer to improve the signal-to-noise ratio and raise the cable frequency response.

c. The acceleration signal should be digitally integrated. The following improved routine may be used to advantage. First, high pass filter the acceleration data at the desired low frequency cut-off point. Then, integrate the result. If the resultant velocity does not return to zero at the same time the derivative of the acceleration reaches final zero, then adjust the low frequency cut-off point up or down the spectrum accordingly.

The development effort here also suggests that further work in studying the accelerometer response is needed. If the path taken by the zero level shift in the accelerometer is predictable, it may be removed to obtain more accurate velocity data.

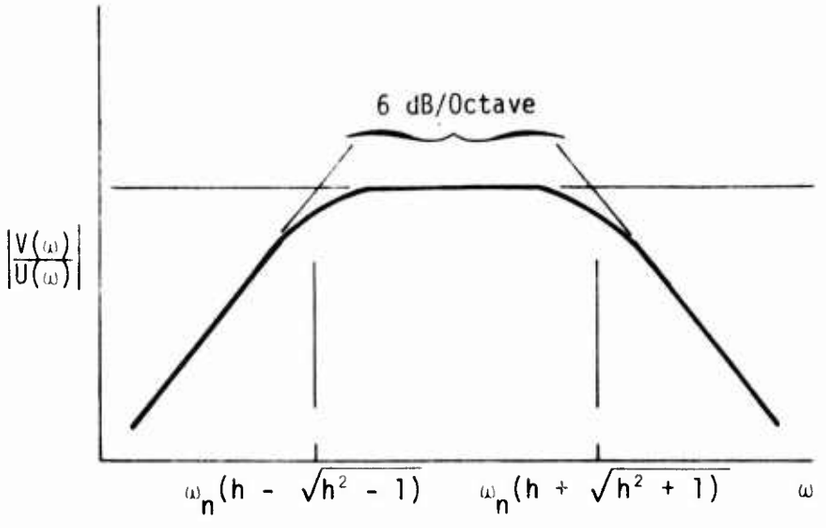

(a) AMPLITUDE

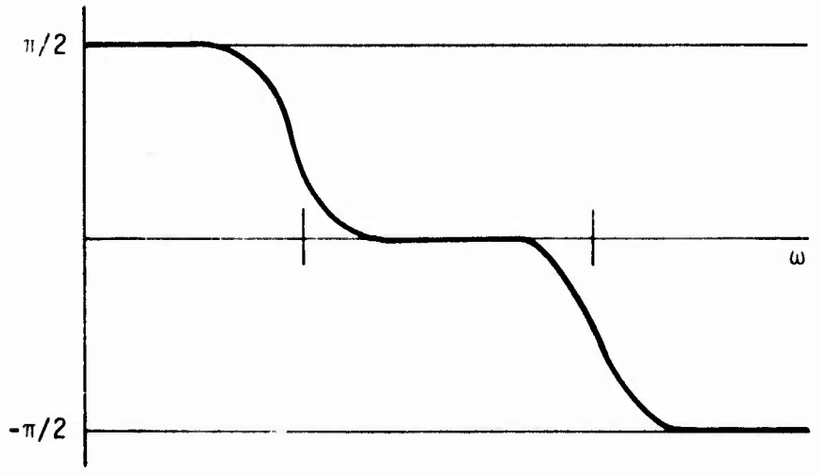

(b) PHASE

Figure 1. Velocity Gage Response

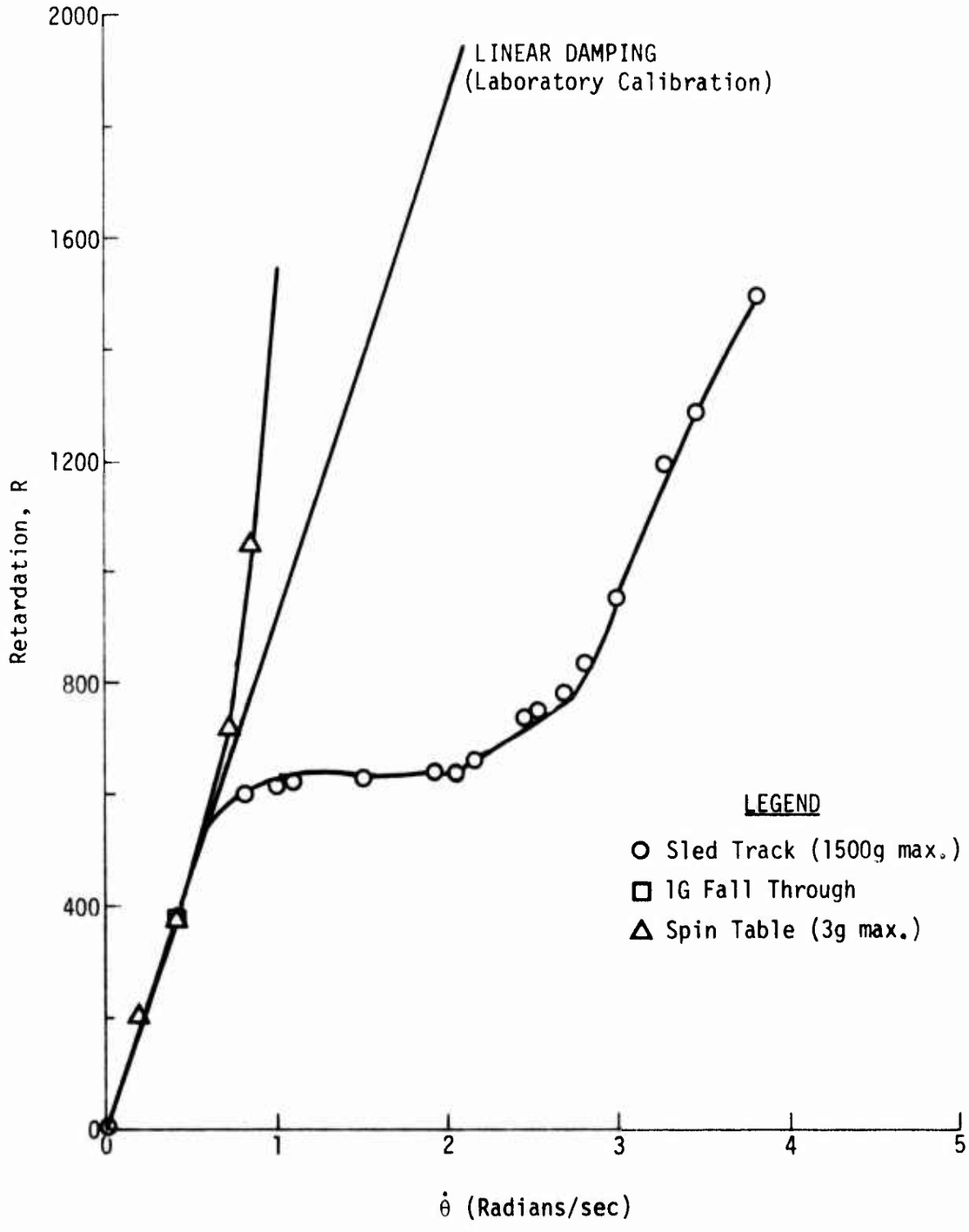

Figure 2. Nonlinear Retardation

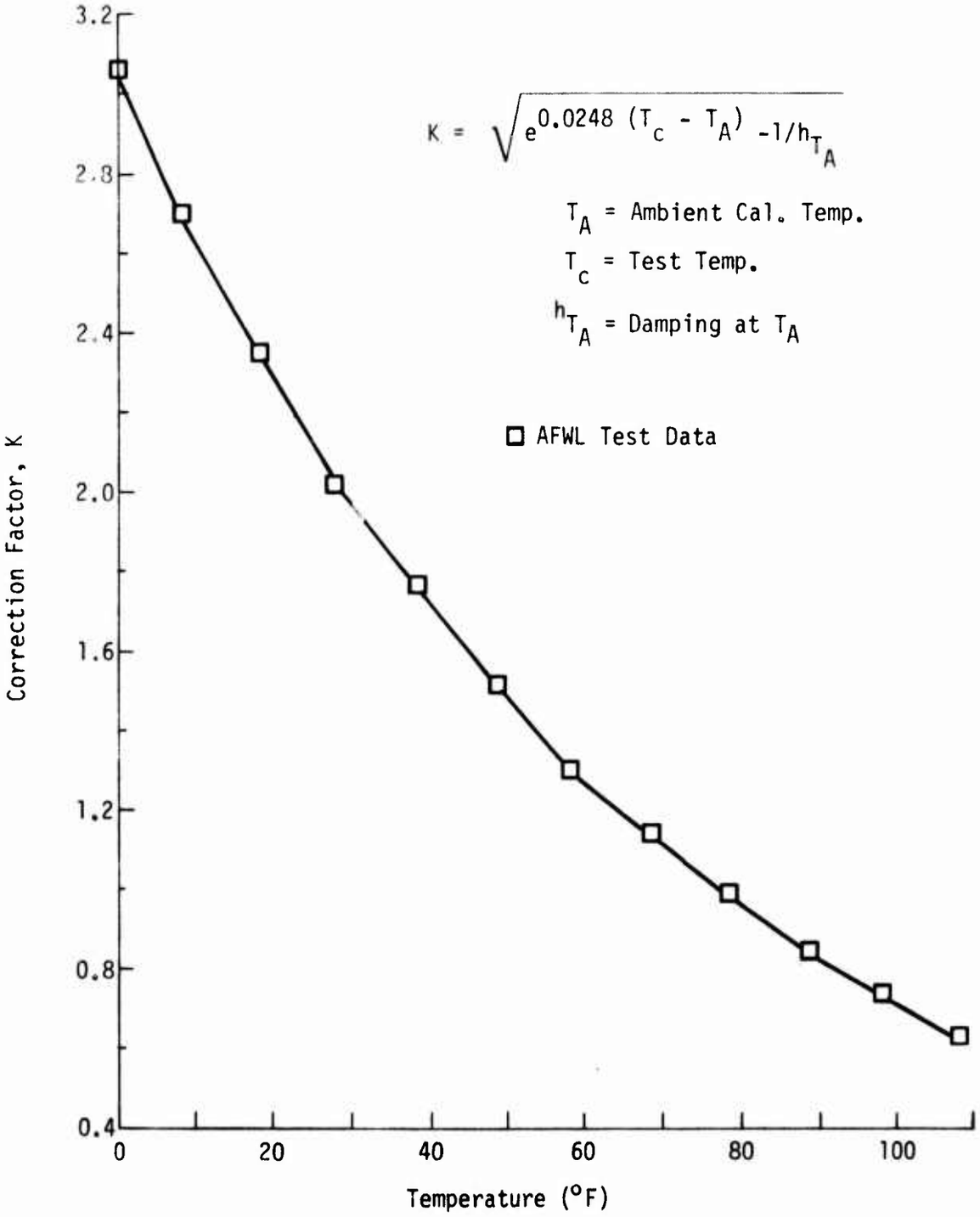

Figure 3. Velocity Gage Temperature Correction Factor

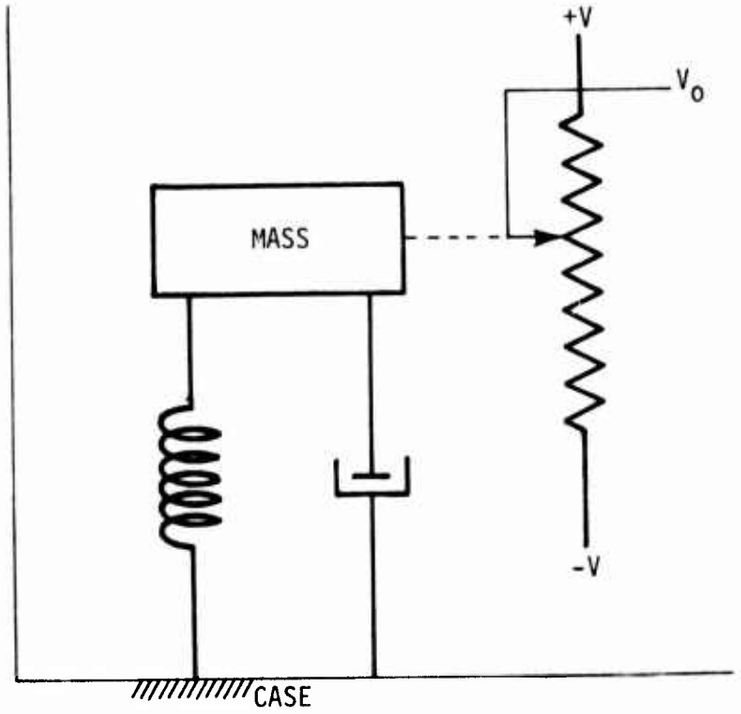

Figure 4. Accelerometer Model

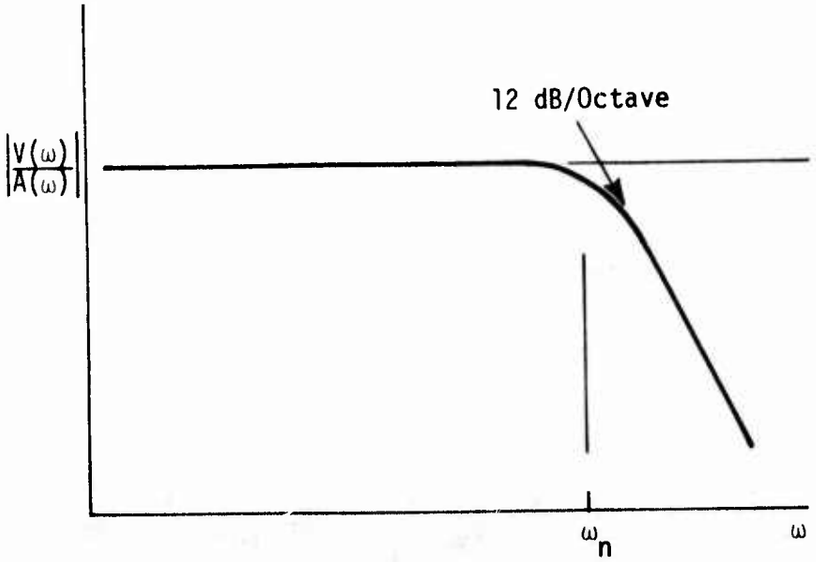

Figure 5. Accelerometer Response

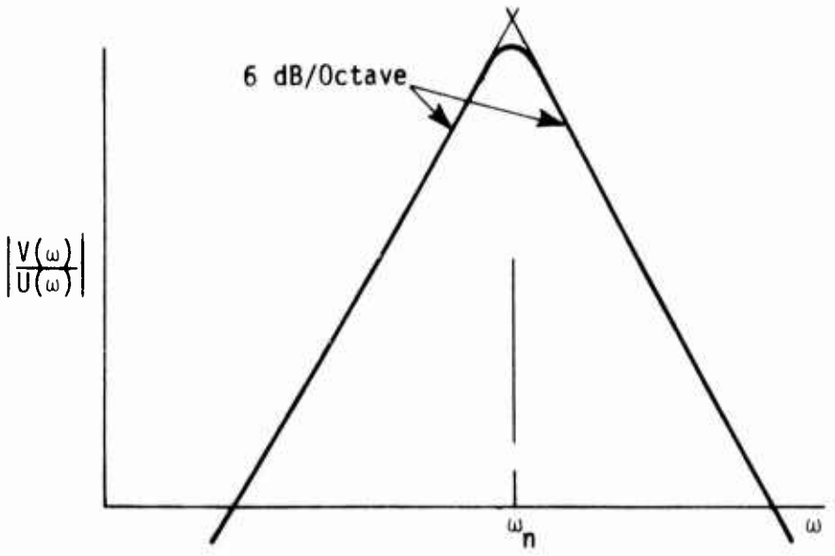

(a) AMPLITUDE

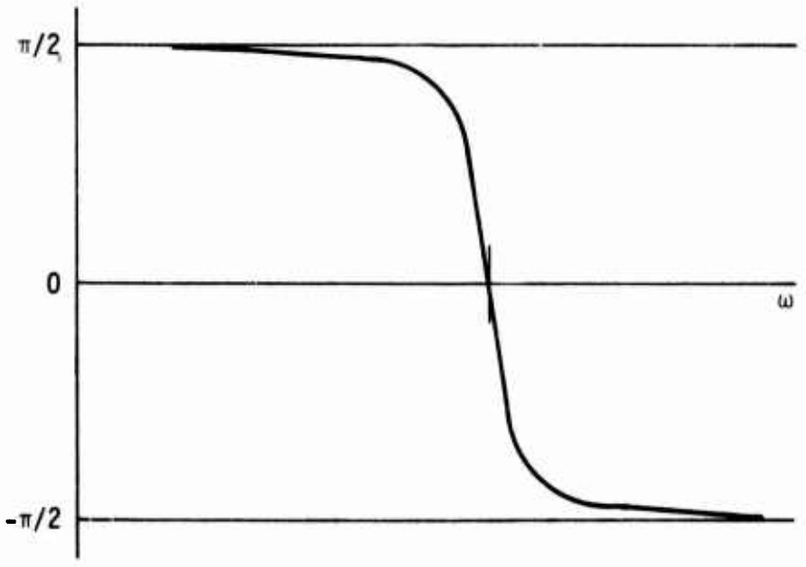

(b) PHASE

Figure 6. Accelerometer Velocity Response

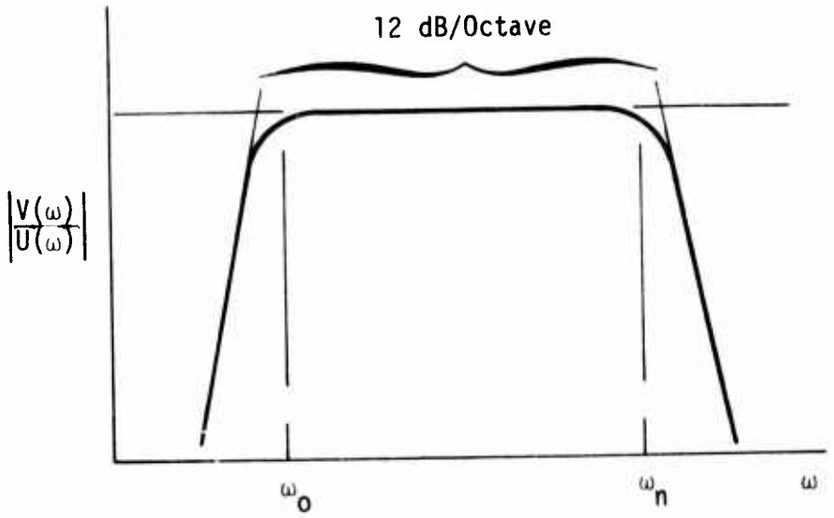

(a) AMPLITUDE

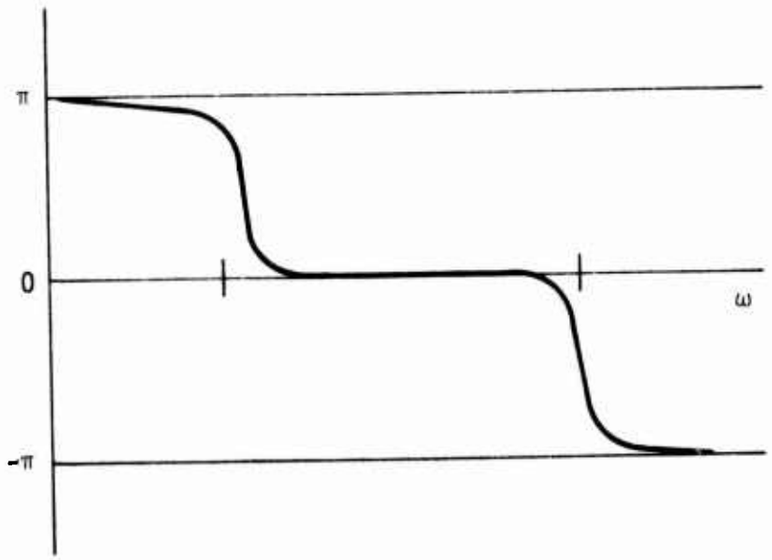

(b) PHASE

Figure 7. Cascaded Response

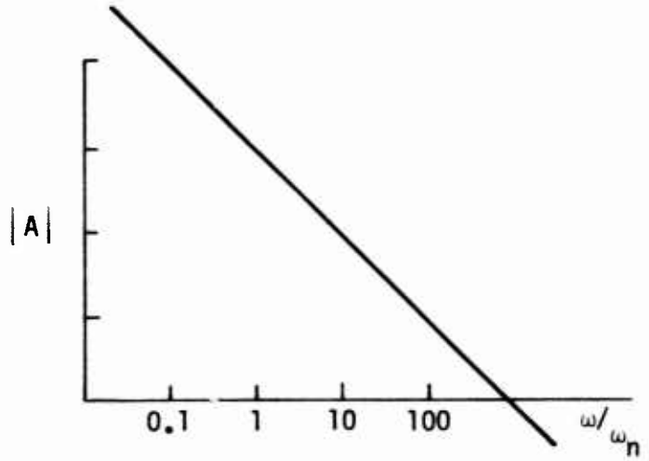

(a) True Integrator Amplitude vs Frequency

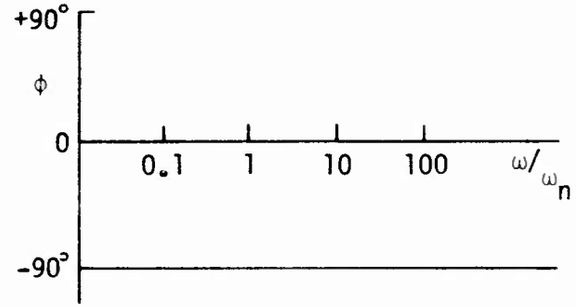

(b) True Integrator Phase vs Frequency

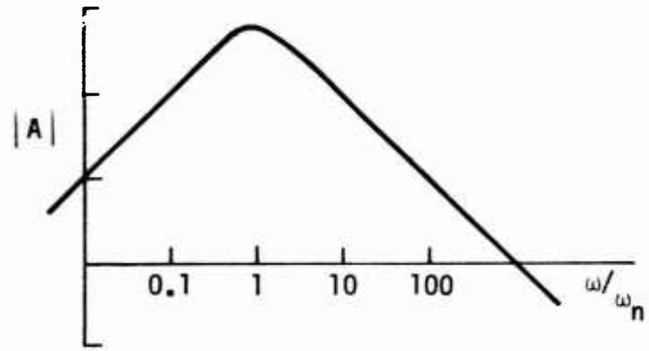

(c) Approximate Integrator Amplitude vs Frequency

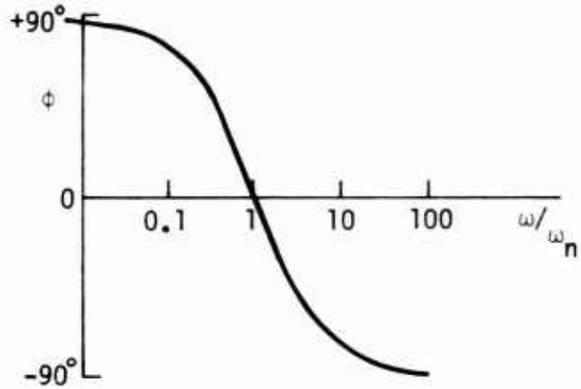

(d) Approximate Integrator Phase vs Frequency

Figure 8. Comparison of True Integrator and Approximate Integrator Responses

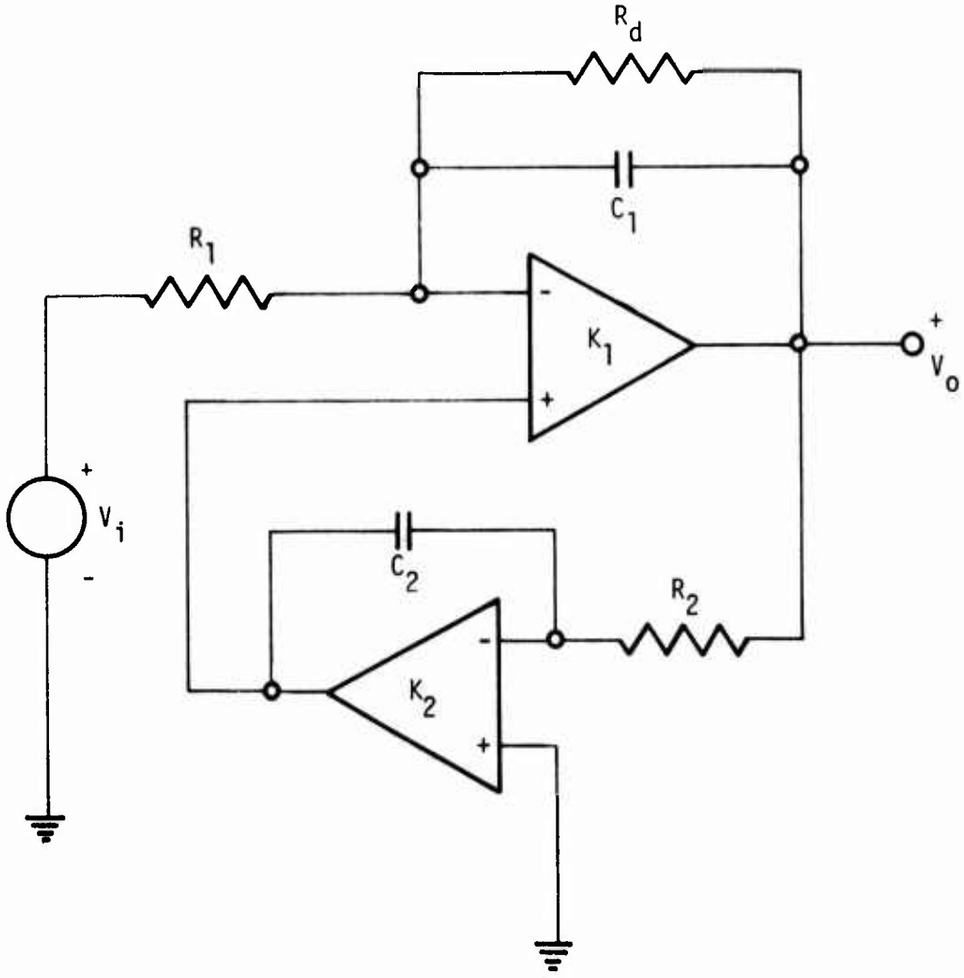

Figure 9. An Approximate Integrating Circuit with Finite Gain Operational Amplifiers

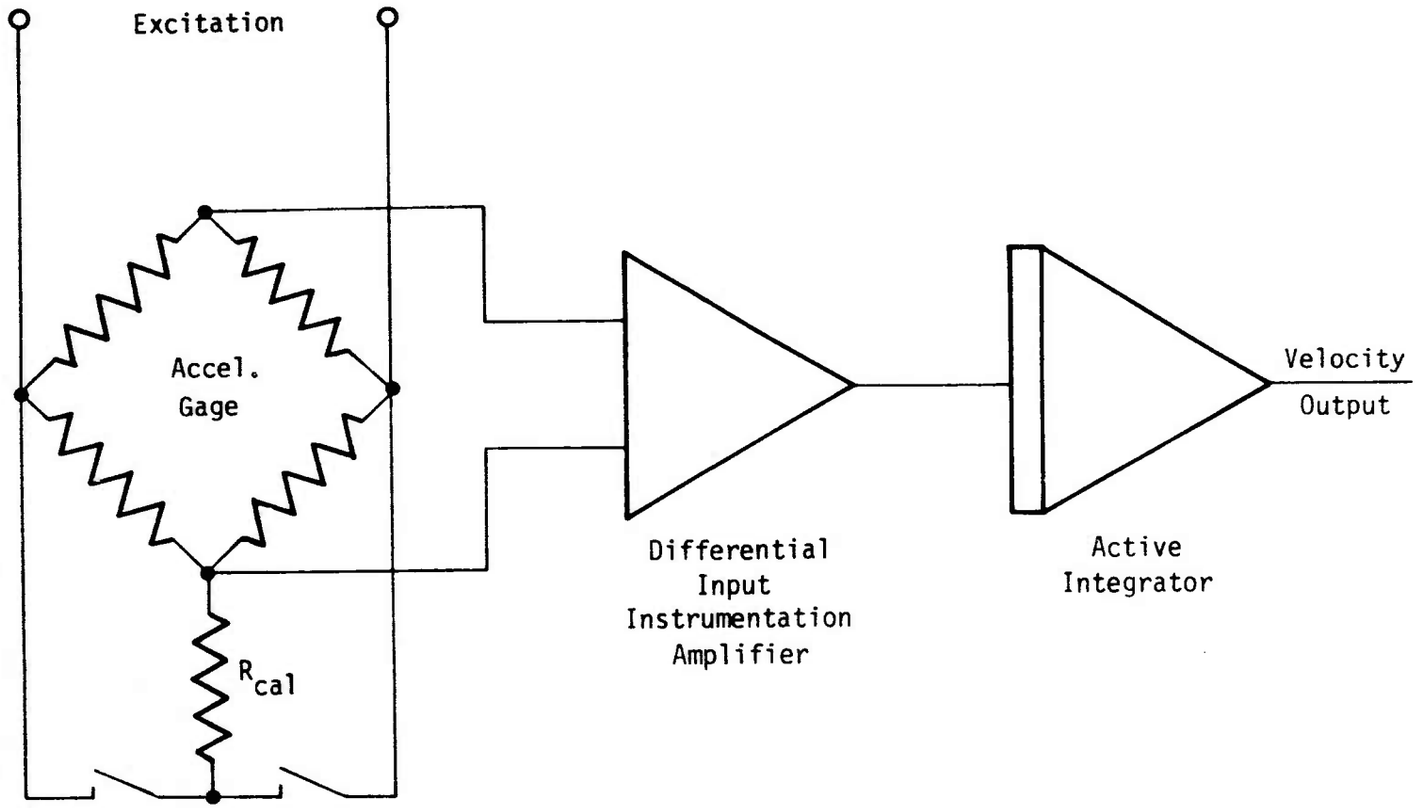

Figure 10. Velocity System

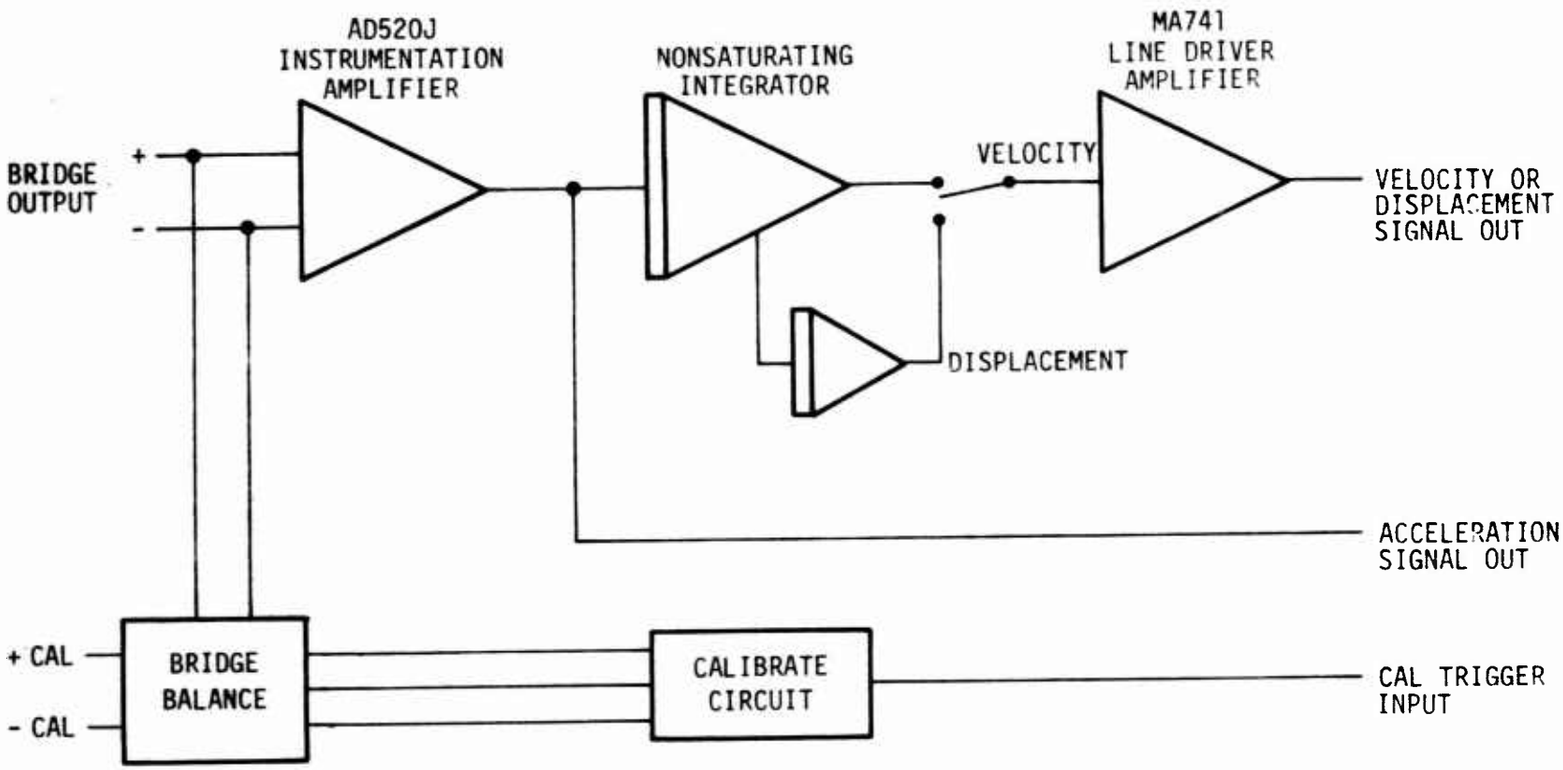

Figure 11. Block Diagram of PACI

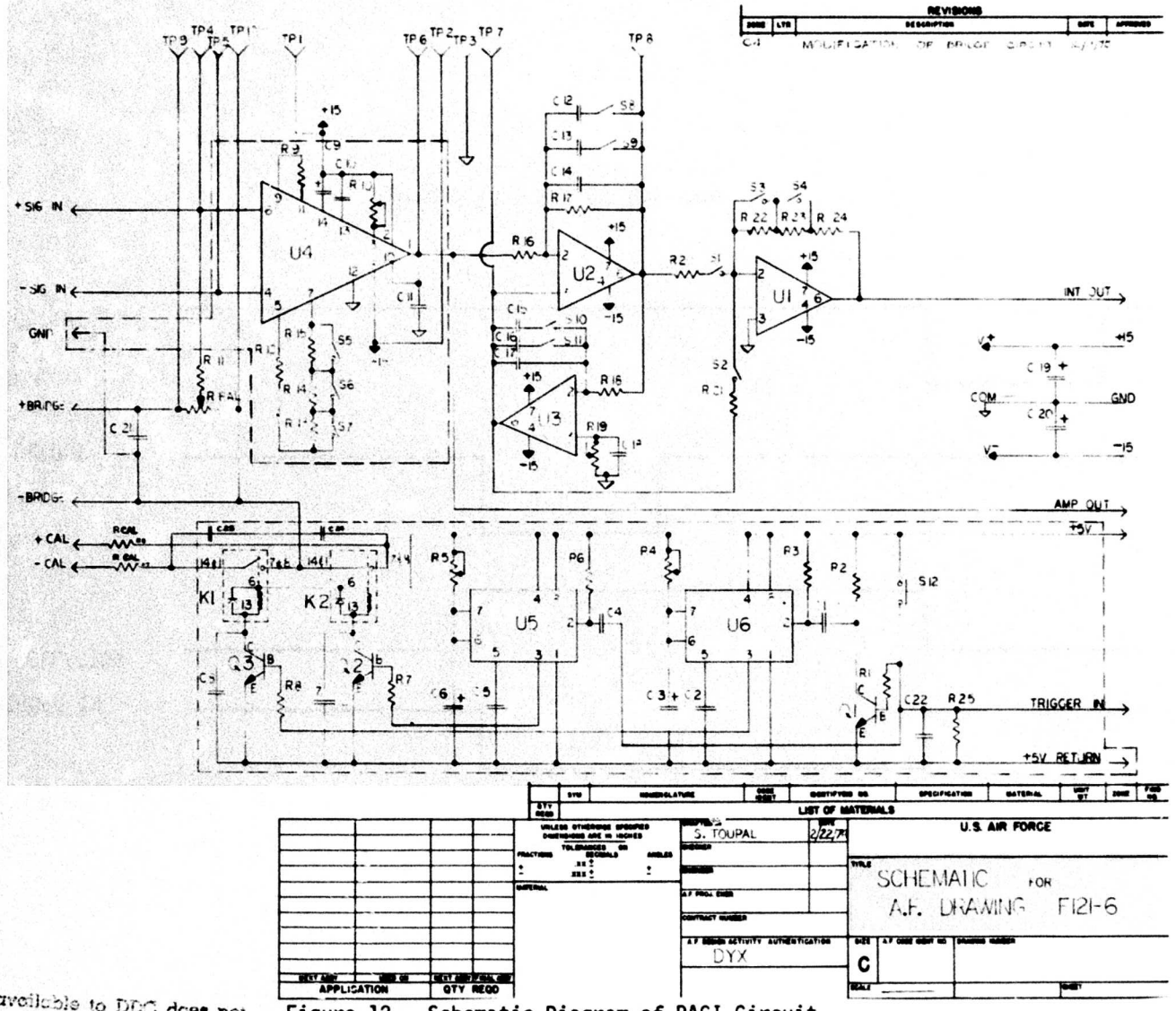

Figure 12. Schematic Diagram of PACI Circuit

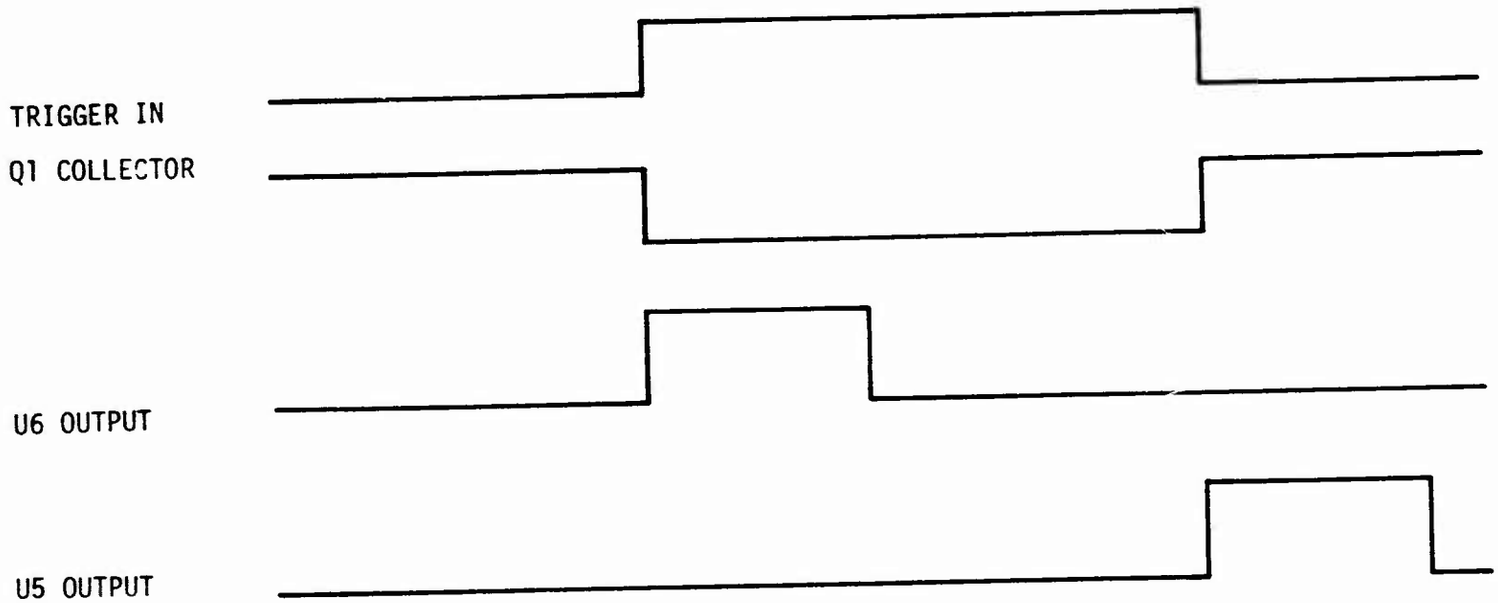

Figure 13. Timing Sequence

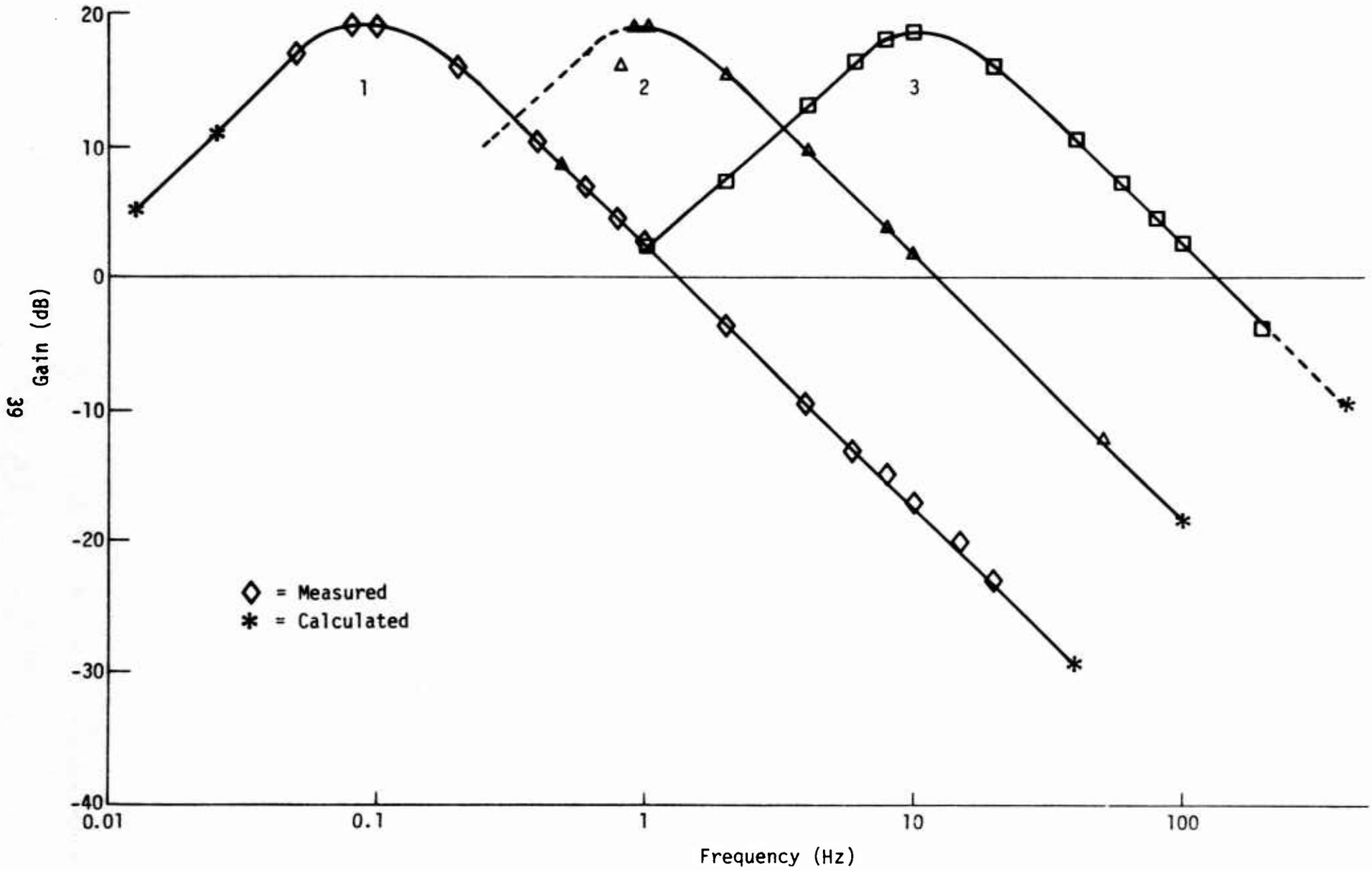

Figure 14. Integrator Frequency Response

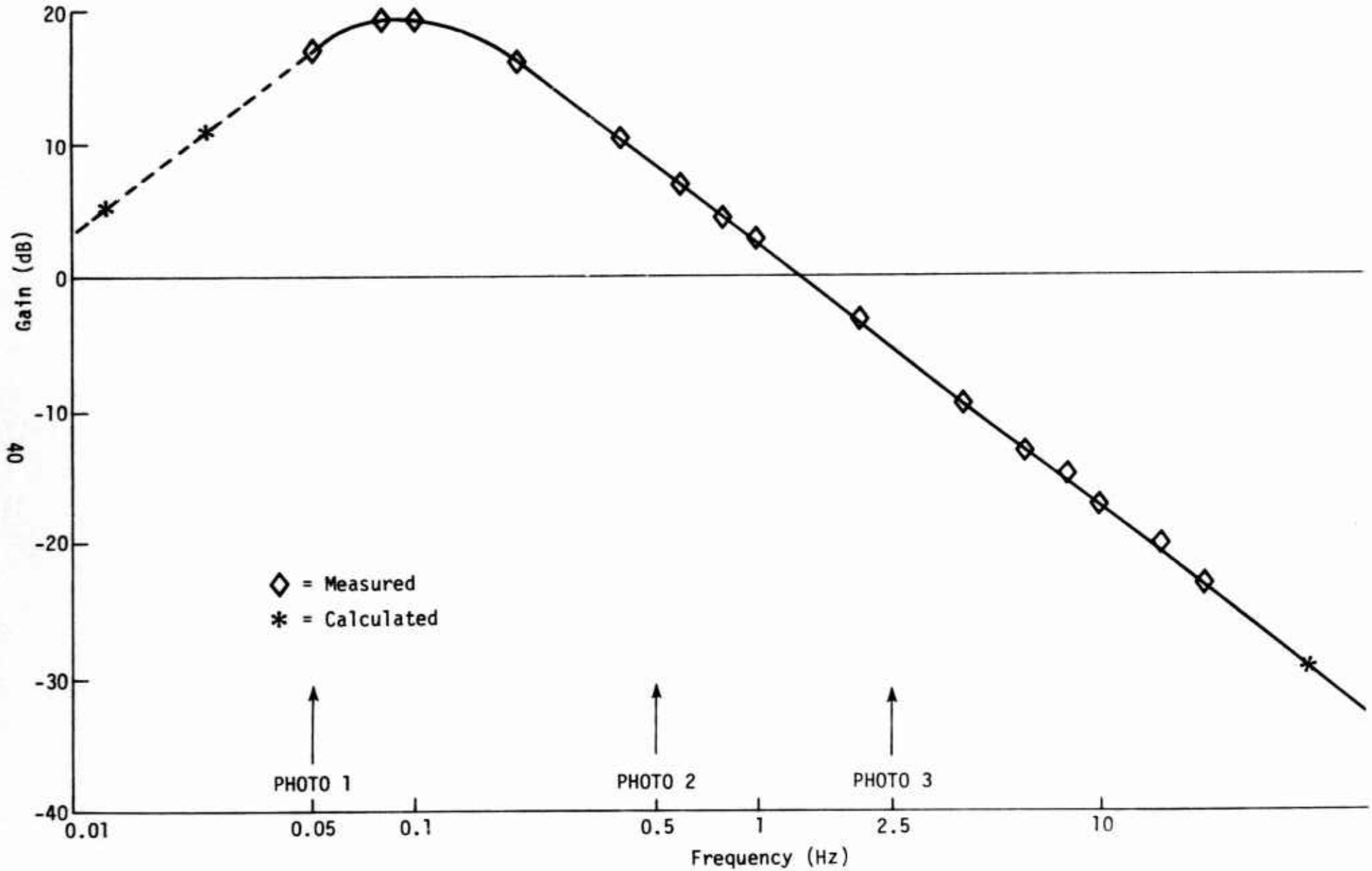

Figure 15. Integrator Frequency Response, Time Constant 1

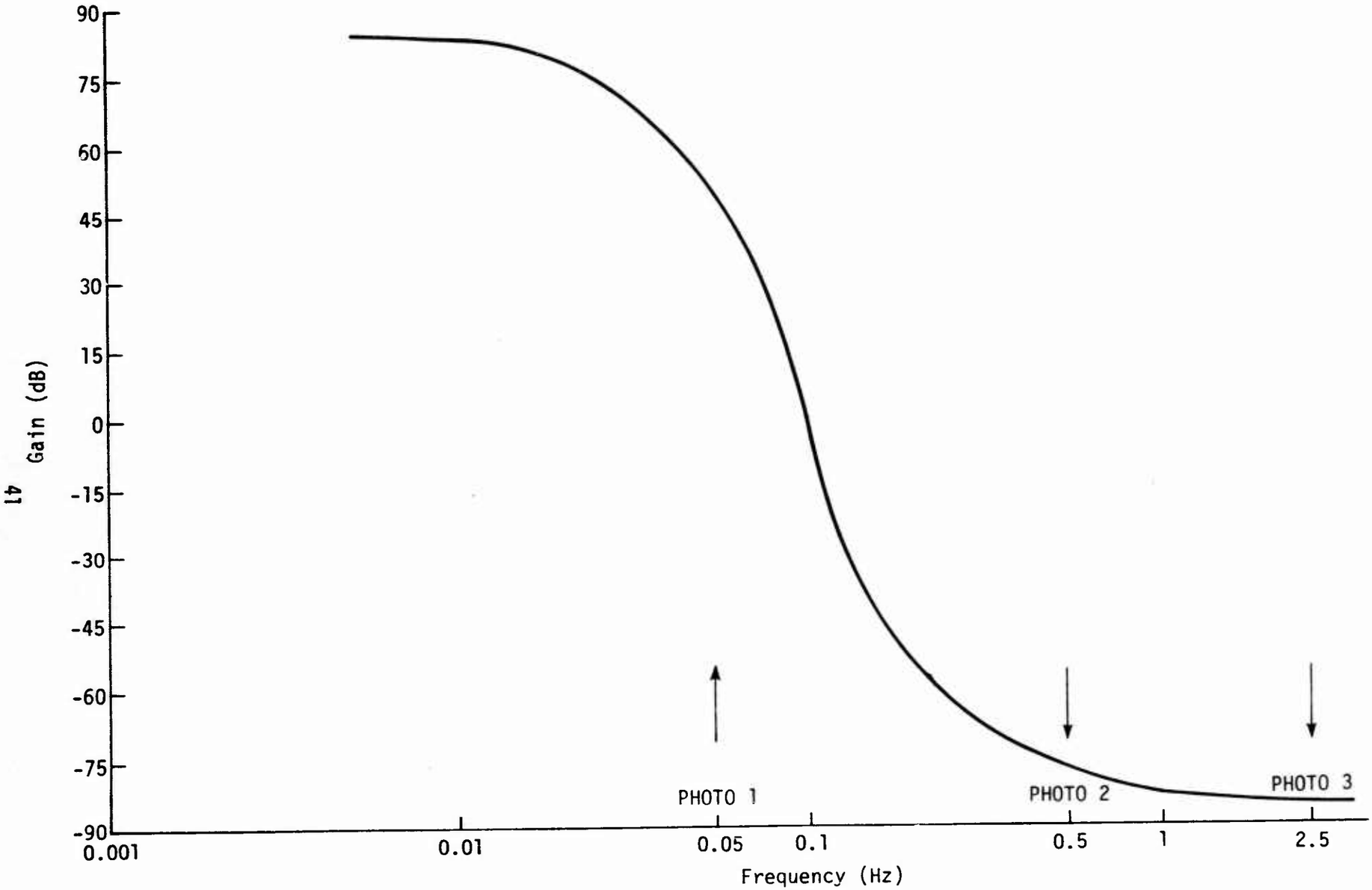

Figure 16. Integrator Frequency Response, Time Constant 1

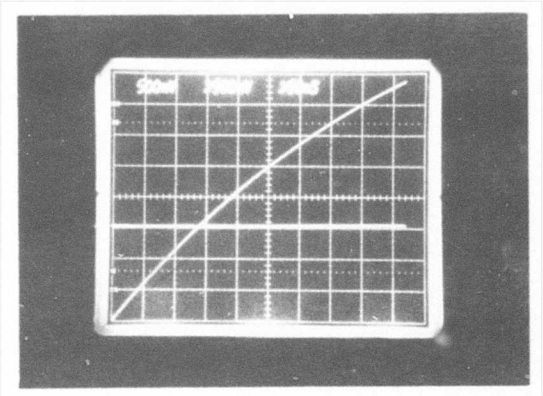

(a) 0.05 Hz

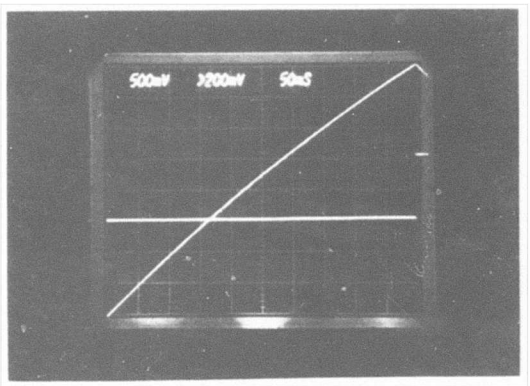

(b) 0.5 Hz

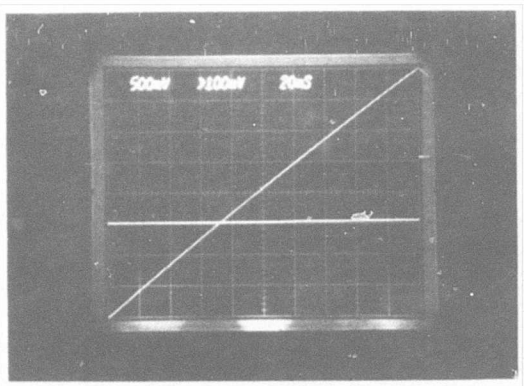

(c) 2.5 Hz

Figure 17. Measured Integrator Output Linearity, Time Constant 1

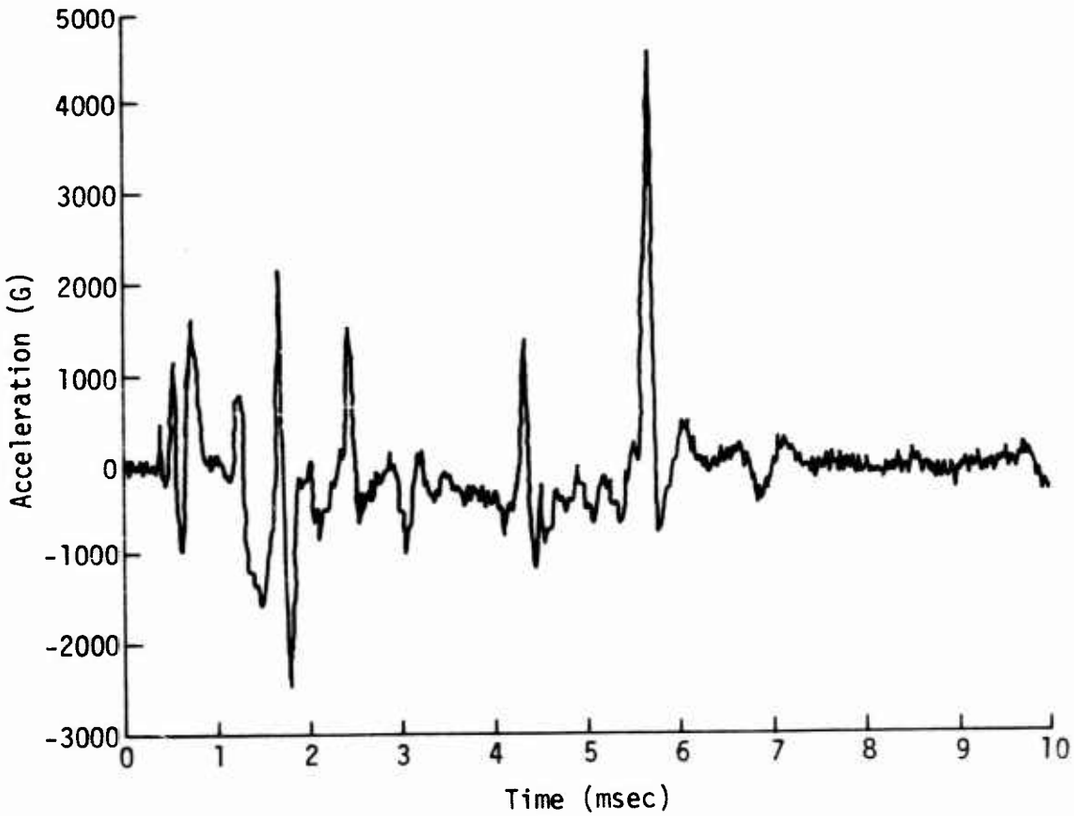

Figure 18. Acceleration (Amplified) versus Time, Gage 1

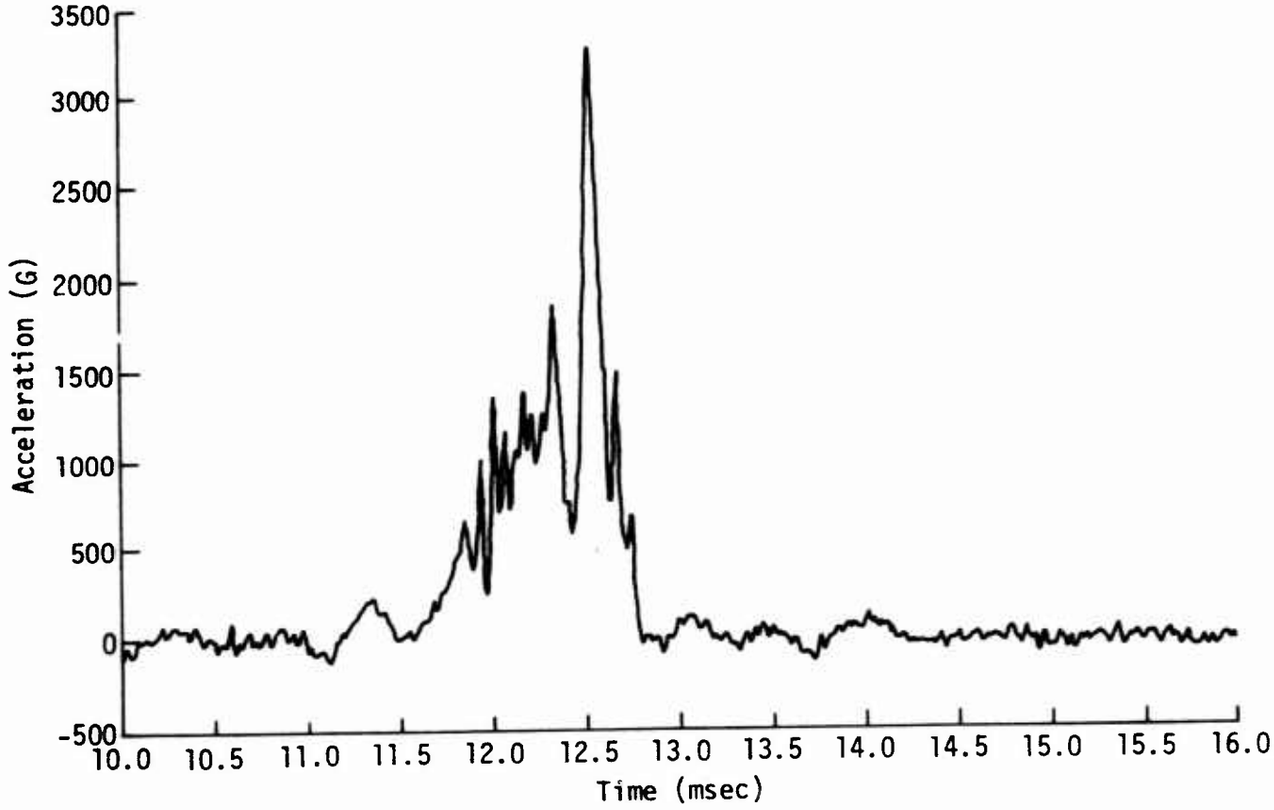

Figure 19. Acceleration (Amplified) versus Time, Gage 2

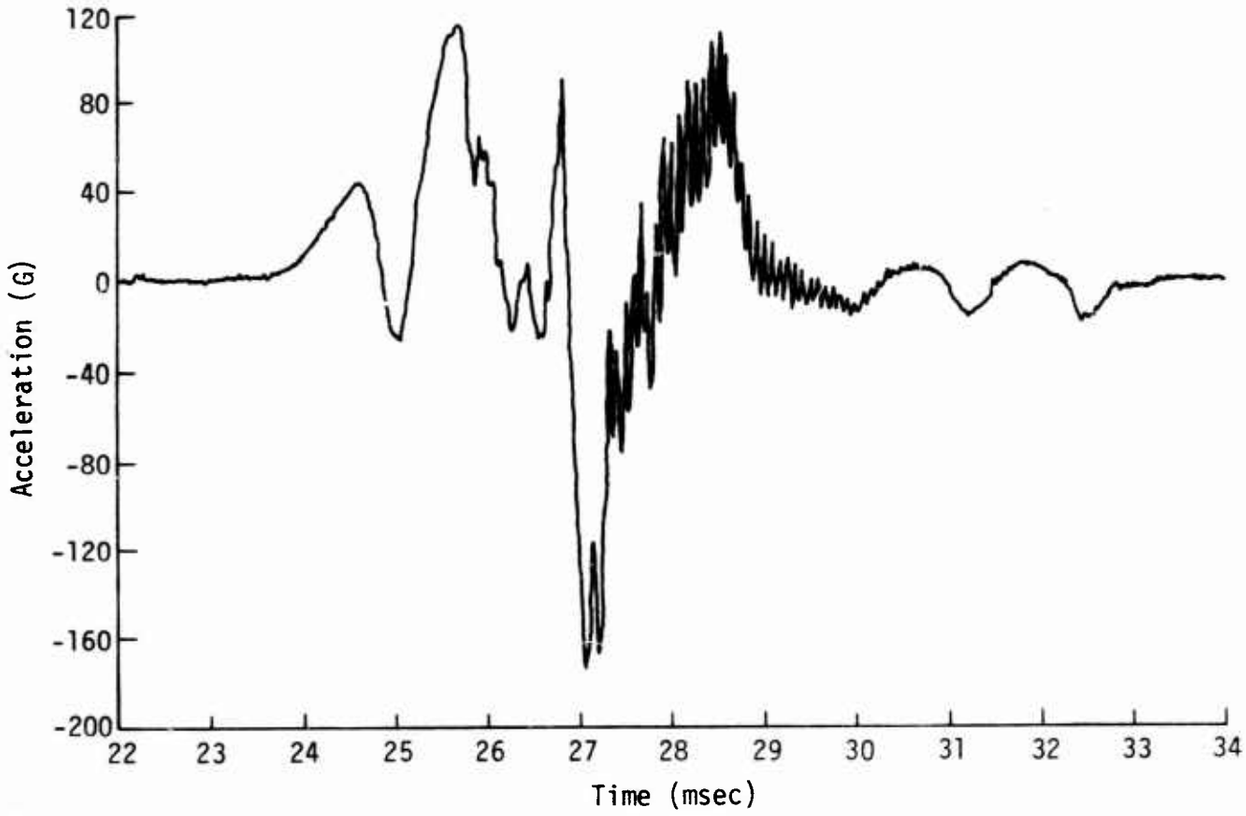

Figure 20. Acceleration (Amplified) versus Time, Gage 4

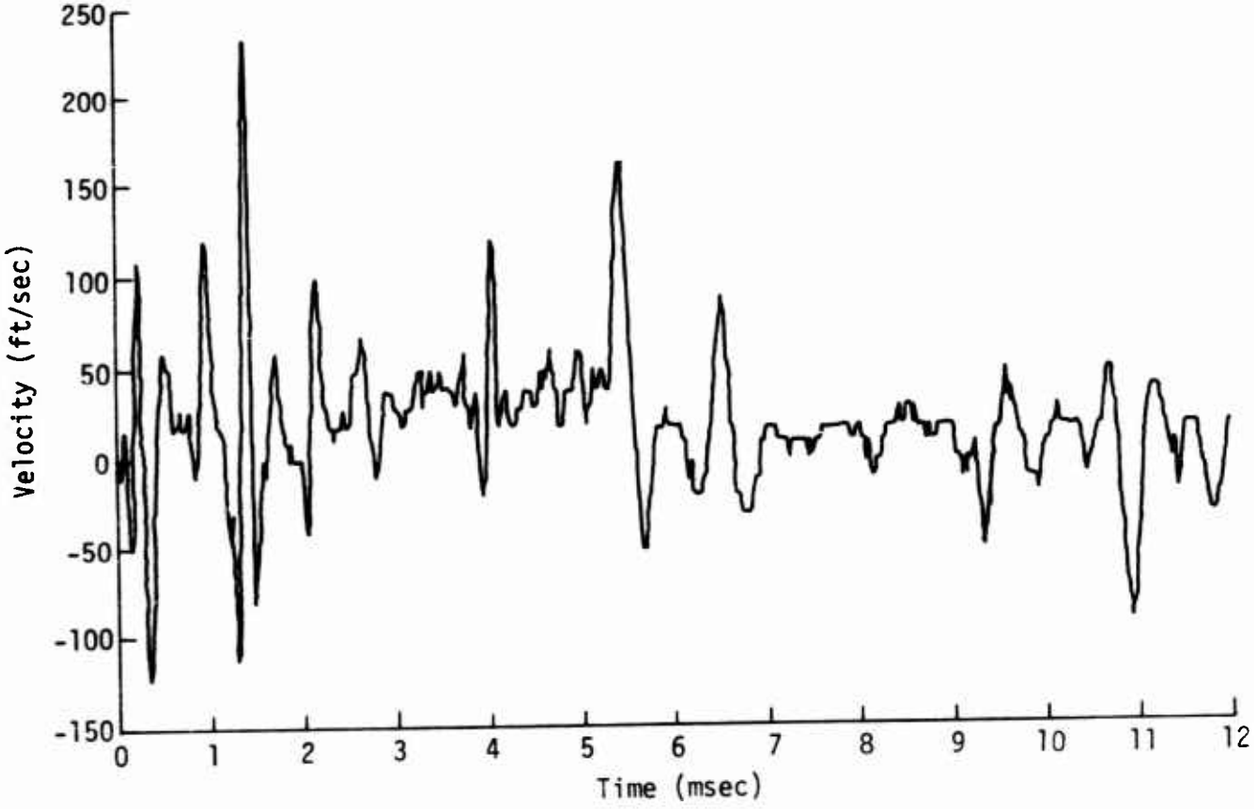

Figure 21. Velocity versus Time, Gage 1, Trace 1

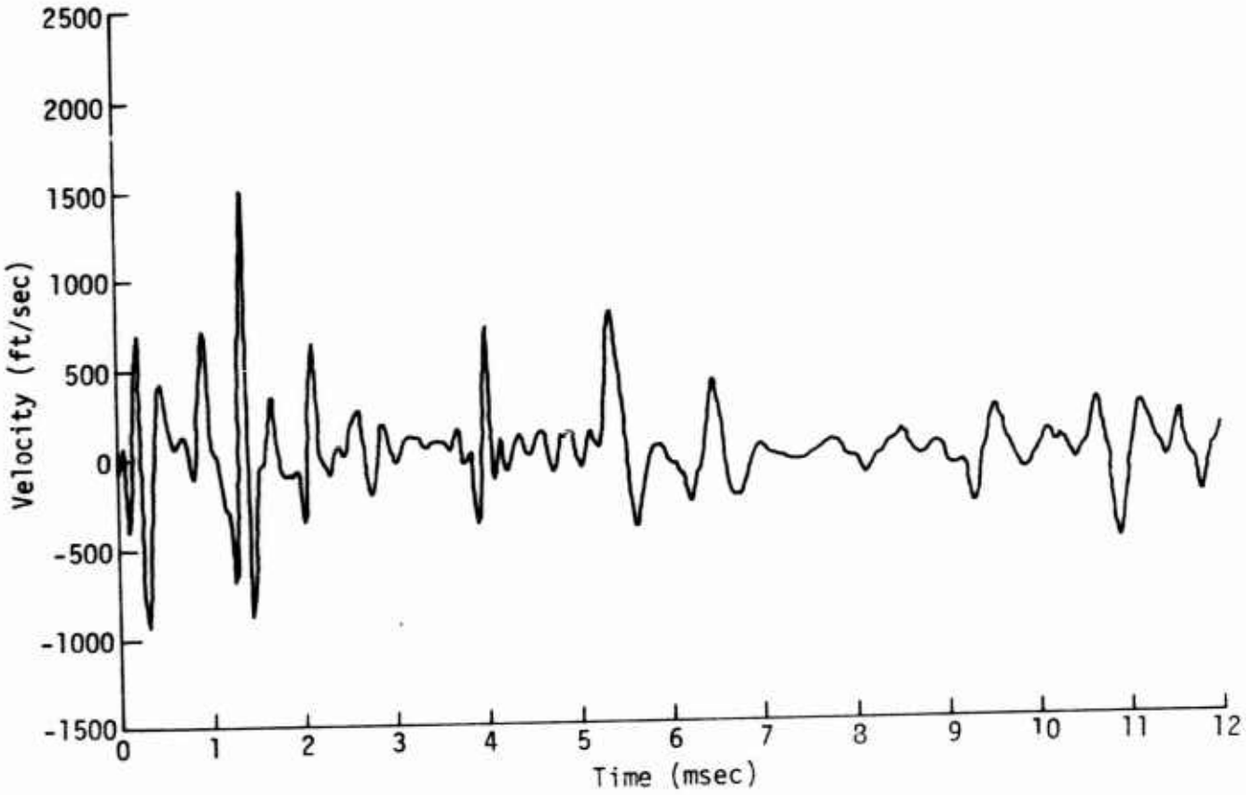

Figure 22. Velocity versus Time, Gage 1, Trace 2

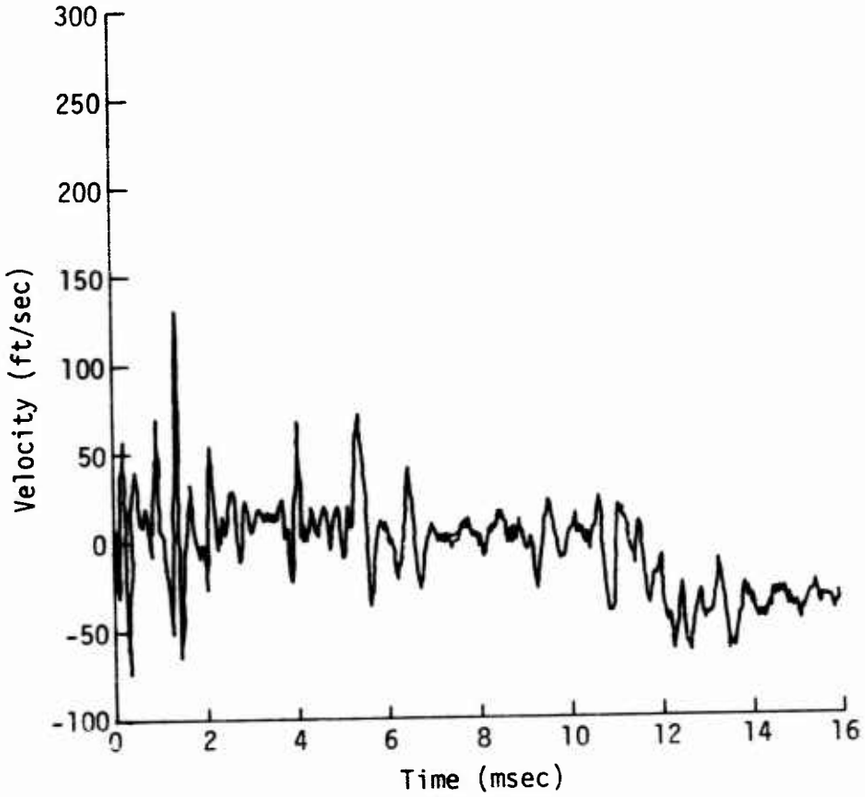

Figure 23. Velocity versus Time, Gage 2, Trace 1

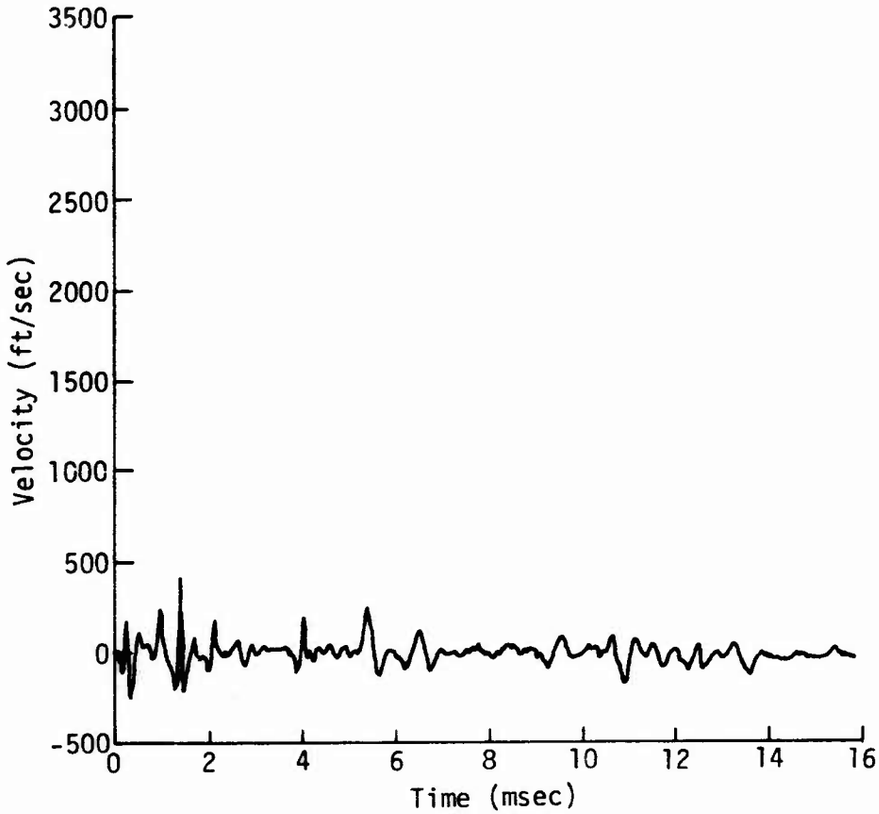

Figure 24. Velocity versus Time, Gage 2, Trace 2

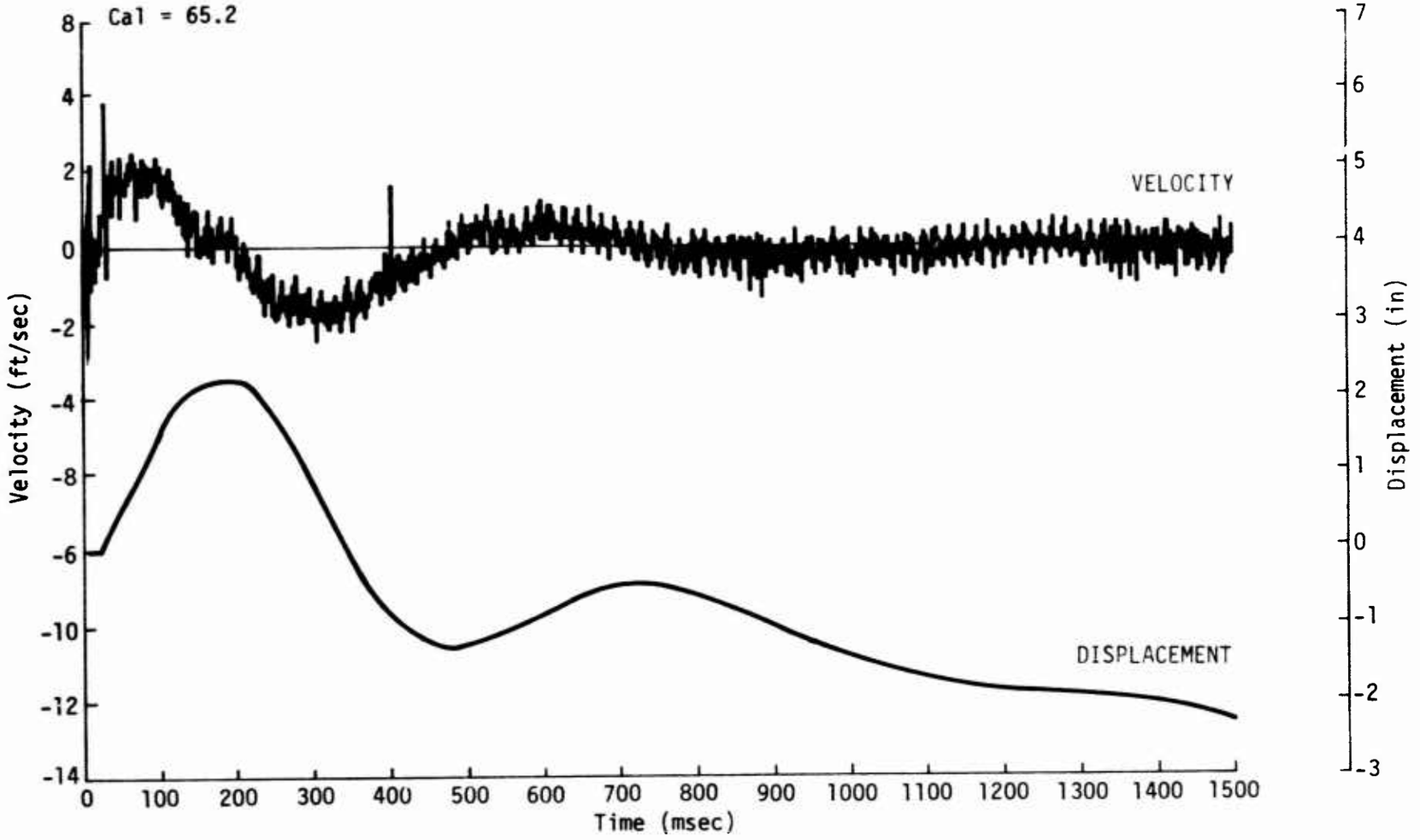

Figure 25. Velocity versus Time, Gage 4, Trace 1

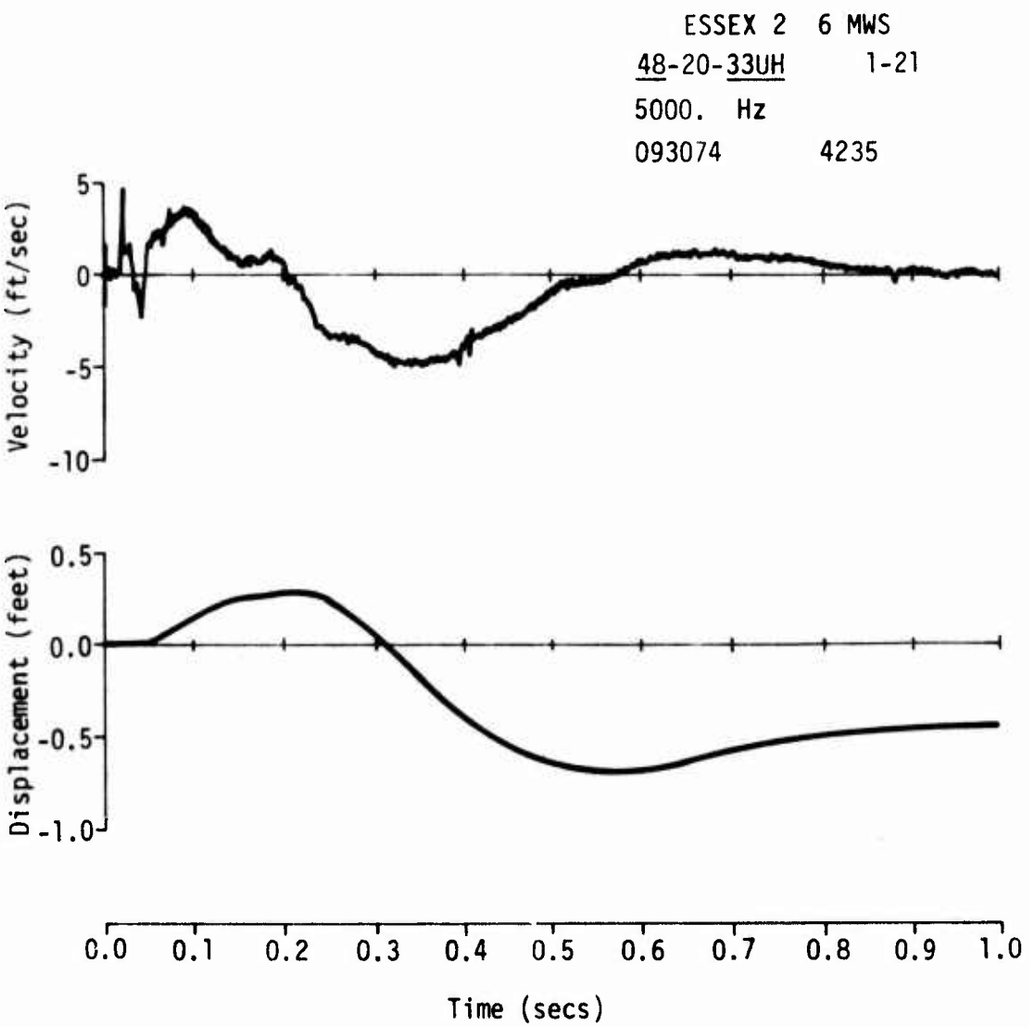

Figure 26. WES Pendulum Gage Data, 48 Meter Station

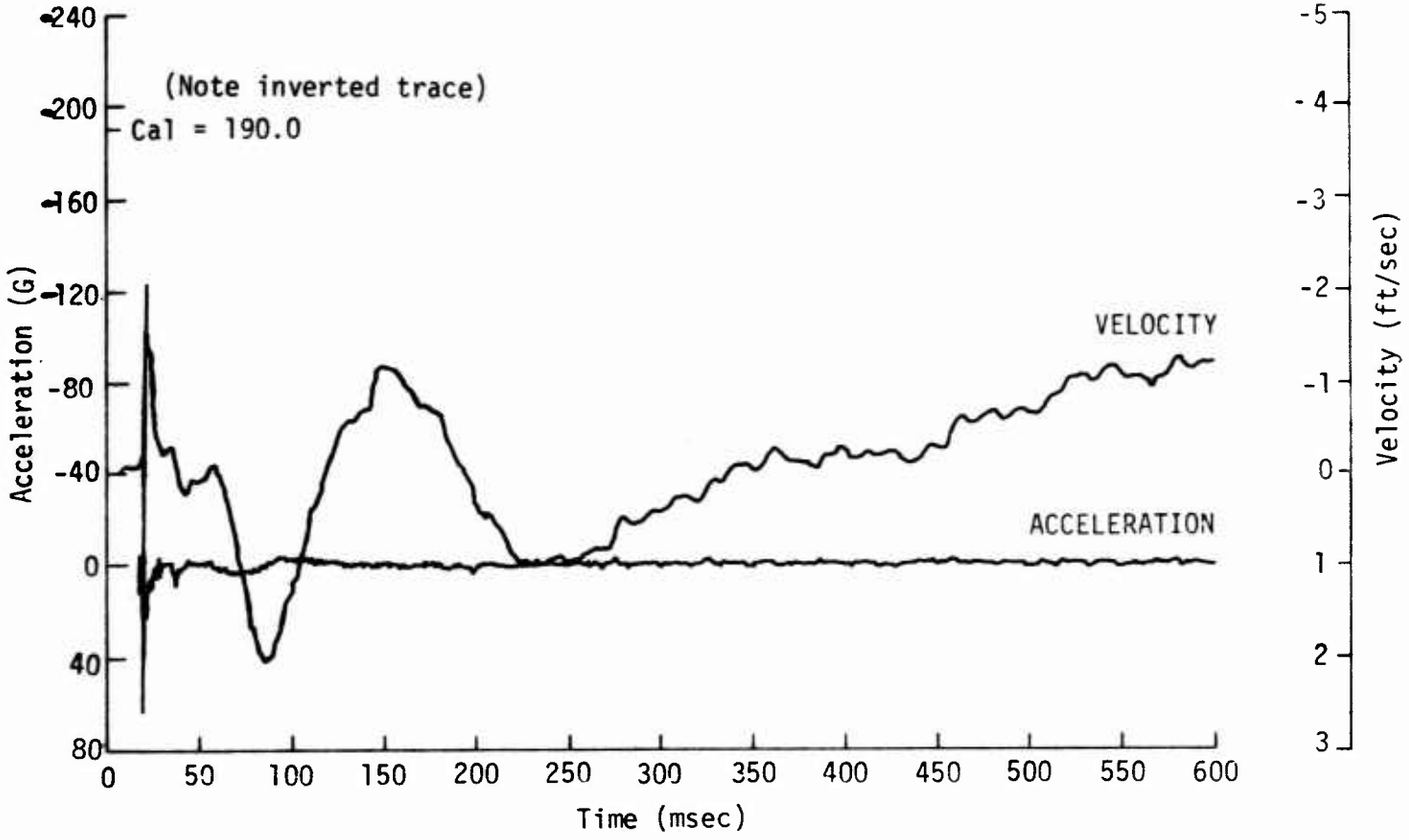

Figure 27. Radial Acceleration and Velocity, Station 5

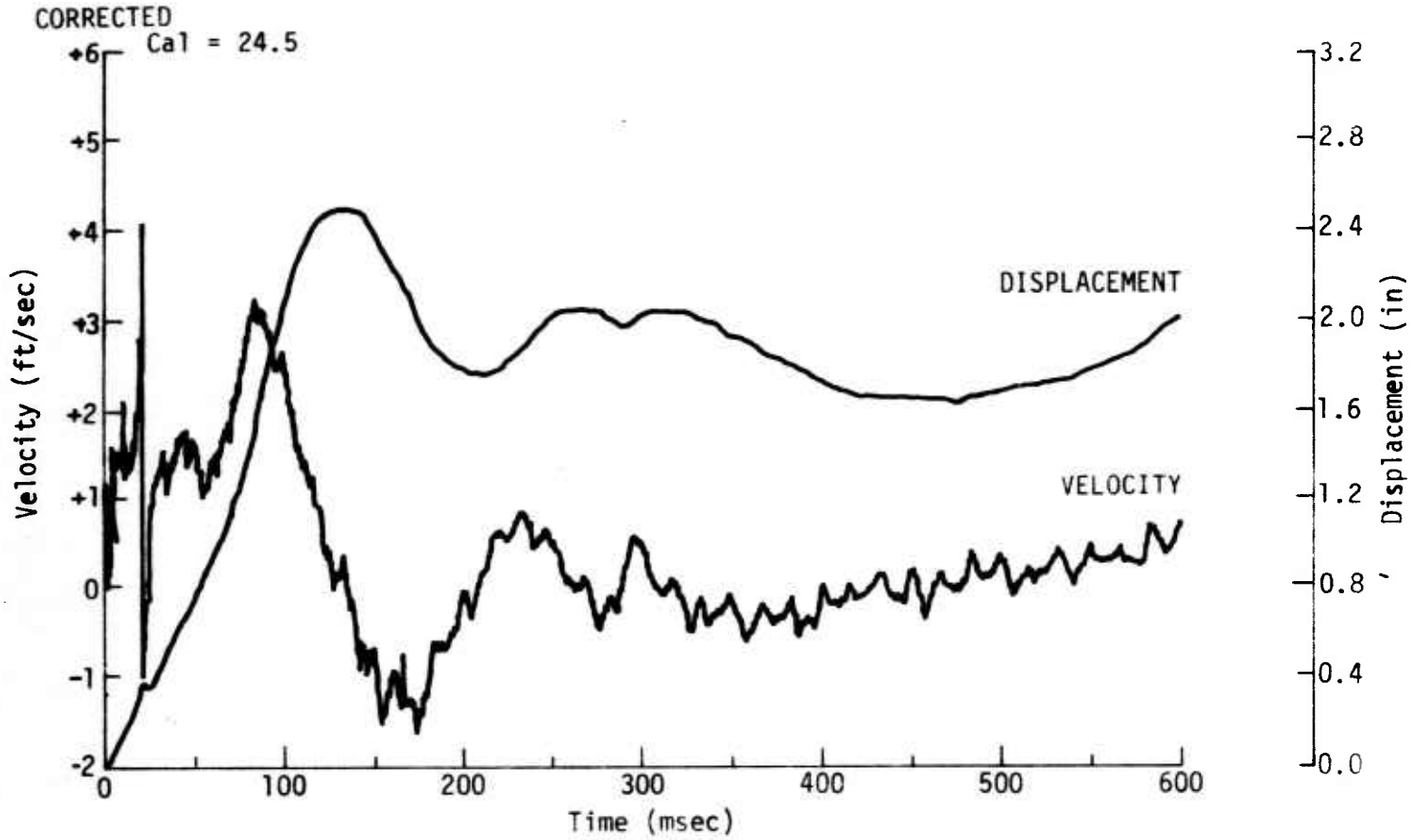

Figure 28. Radial Velocity, Station 5

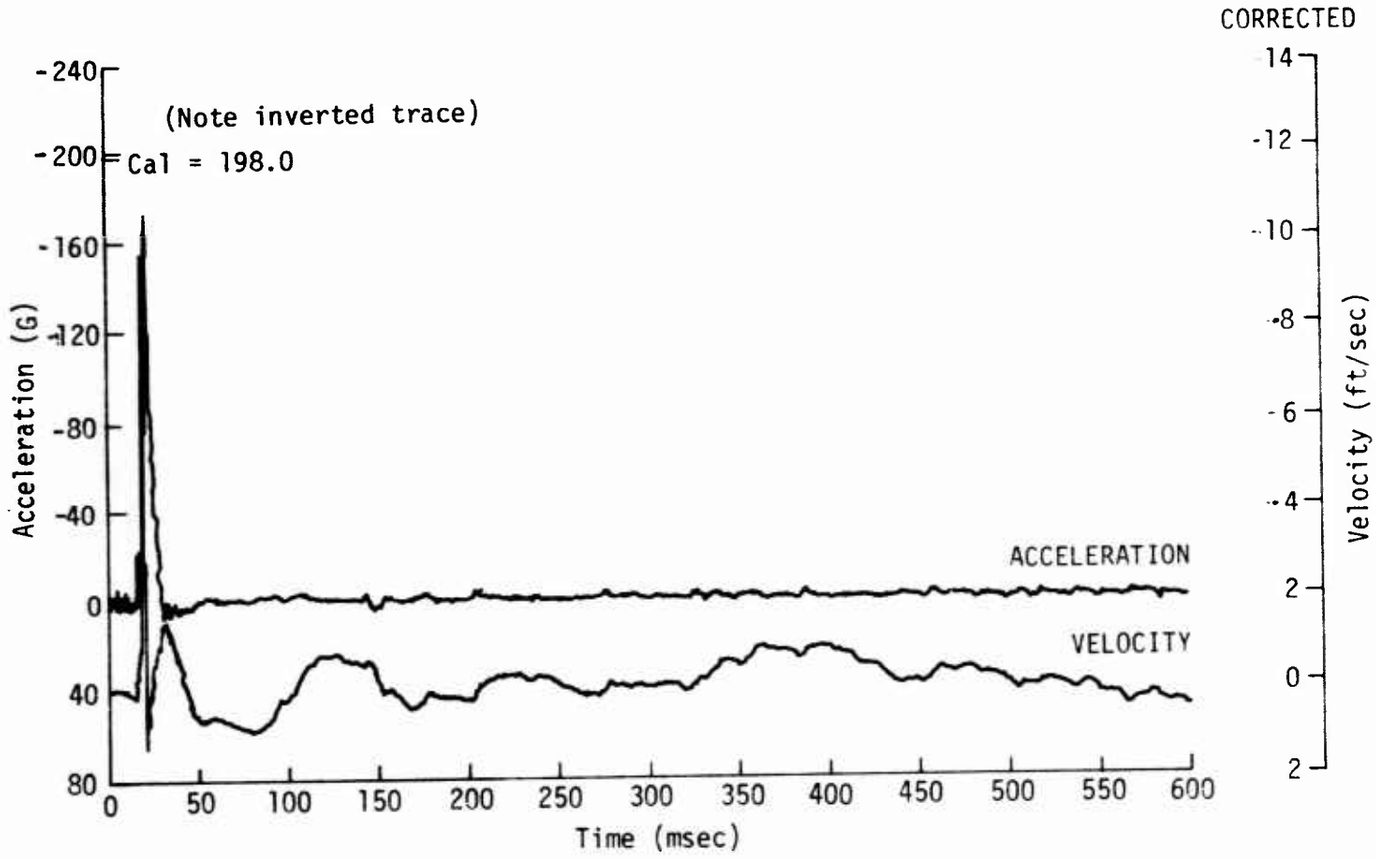

Figure 29. Vertical Acceleration and Velocity, Station 5

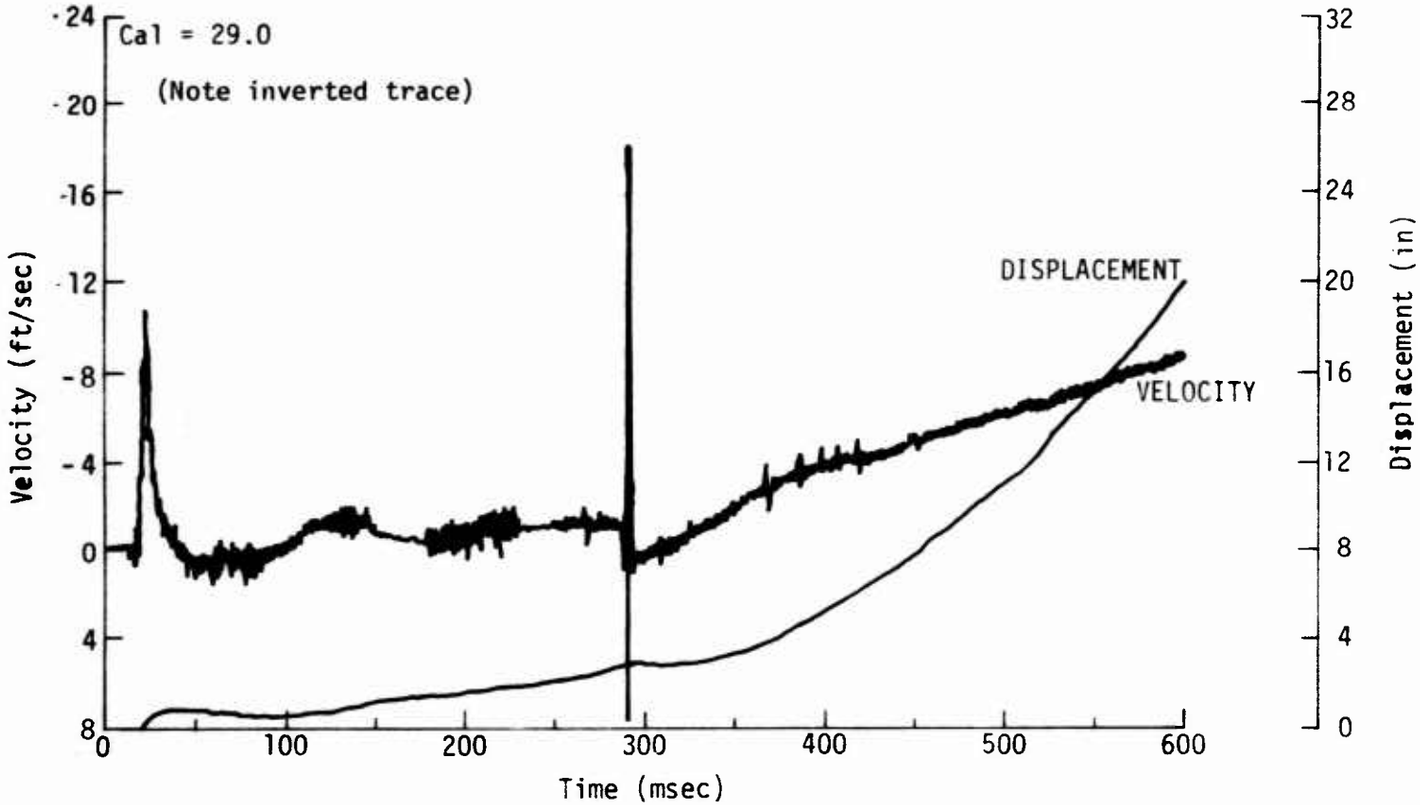

Figure 30. Vertical Velocity, Station 5

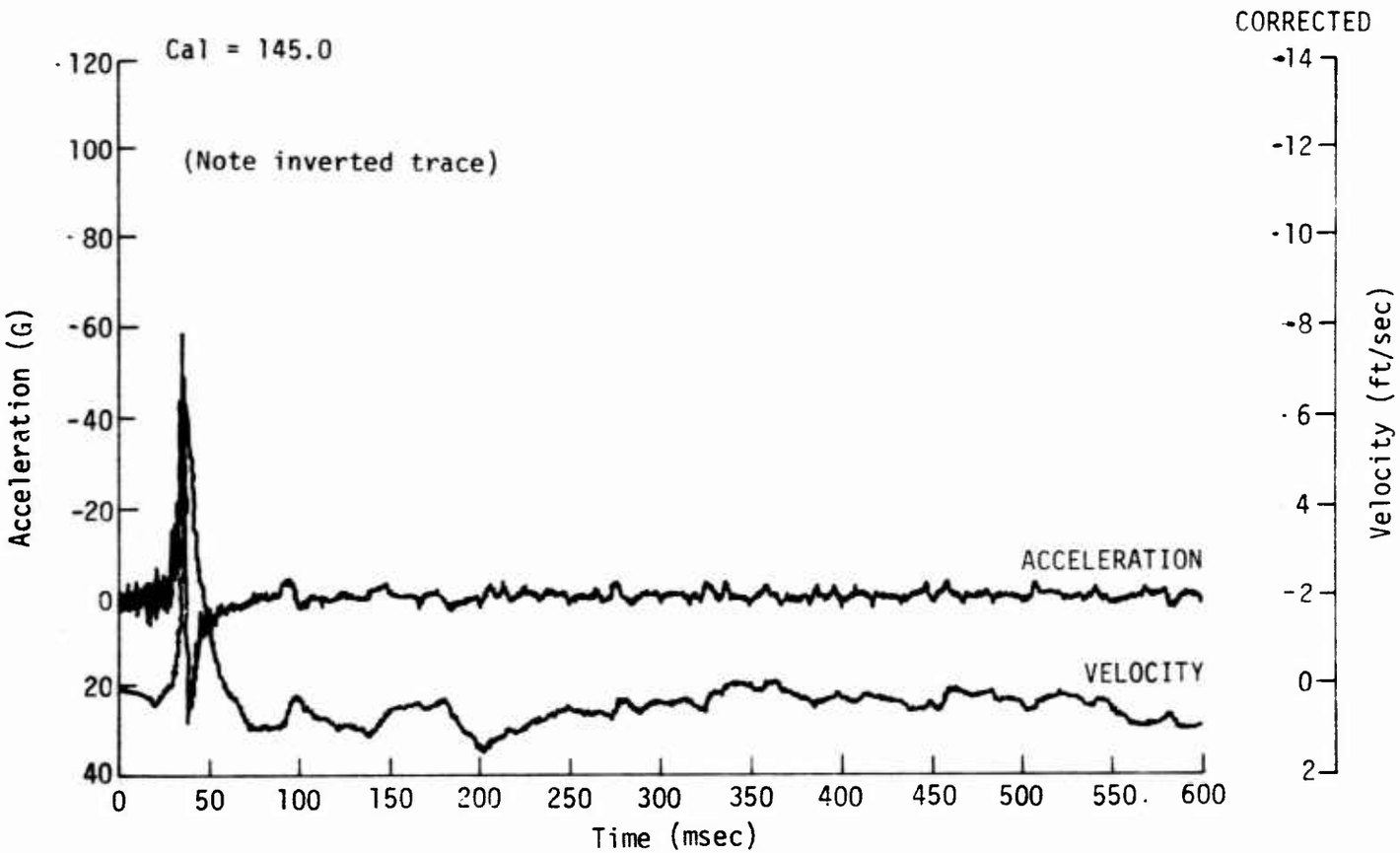

Figure 31. Vertical Acceleration and Velocity, Station 7

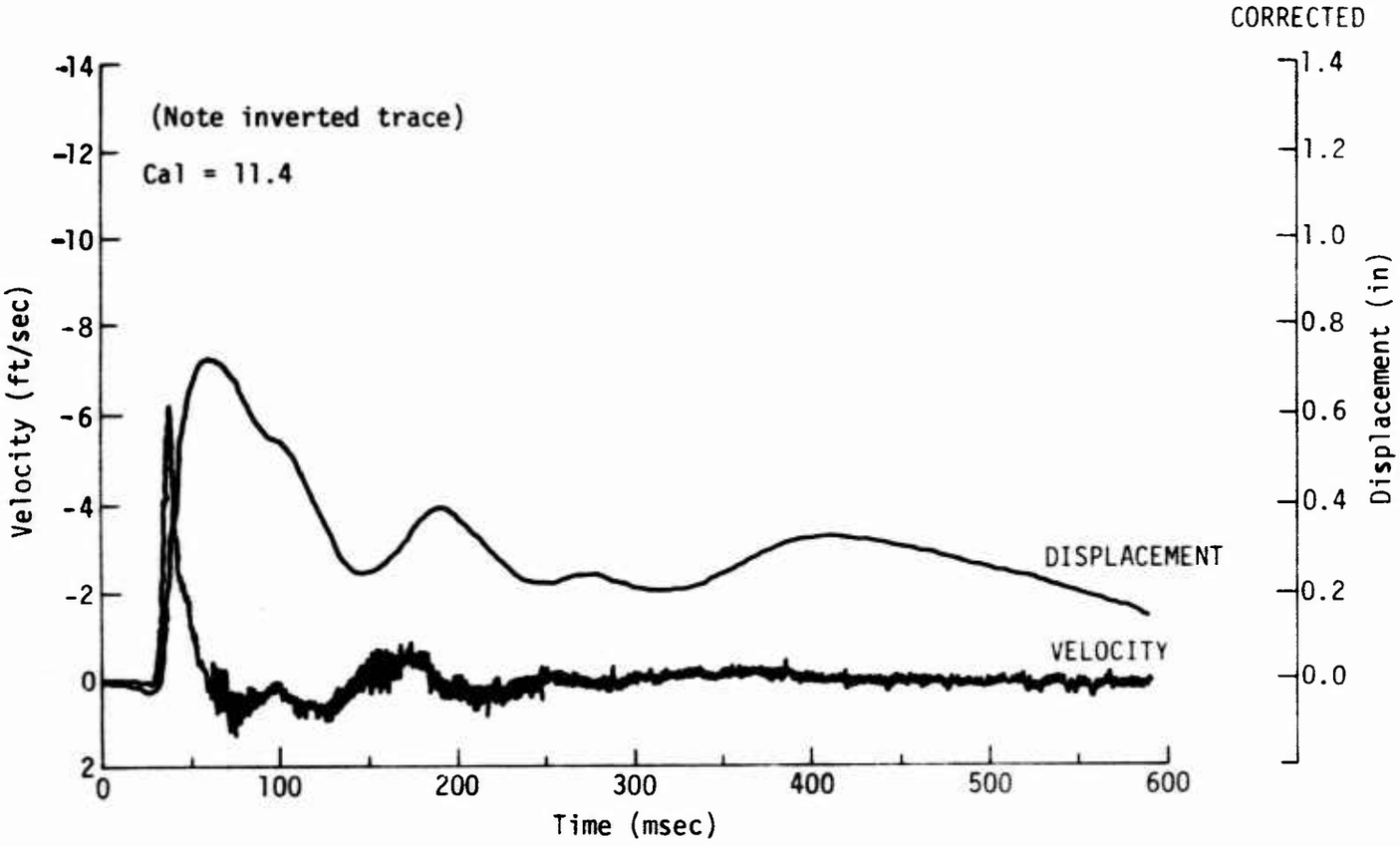

Figure 32. Vertical Velocity, Station 7

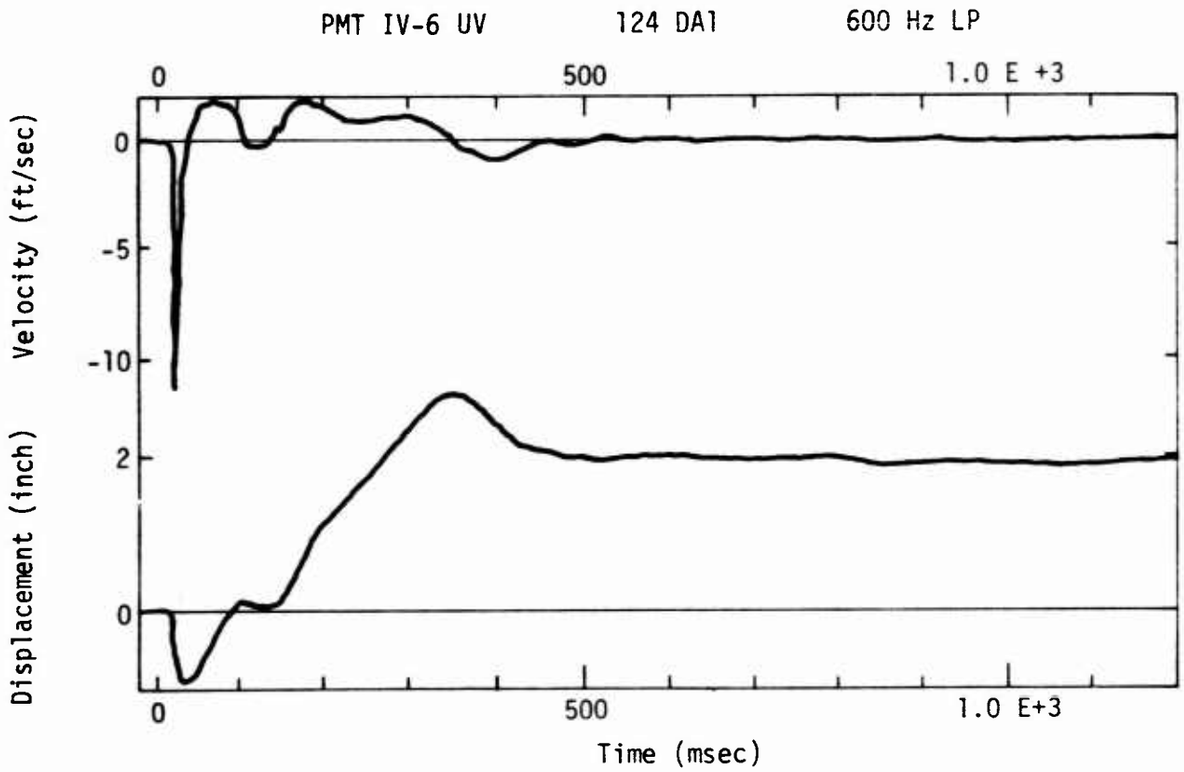

Figure 33. Vertical Ground Motions, Station 5, Bell & Howell Accelerometer

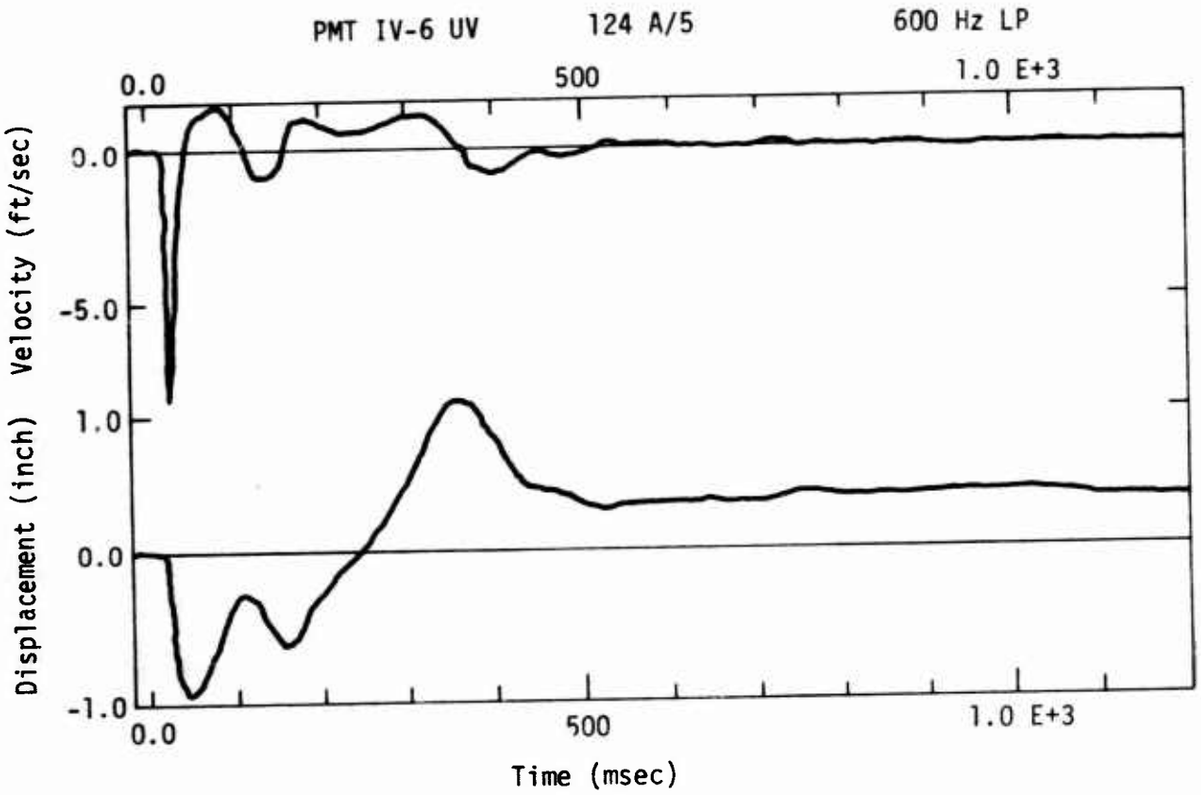

Figure 34. Vertical Ground Motions Pendulum Gage, Station 5

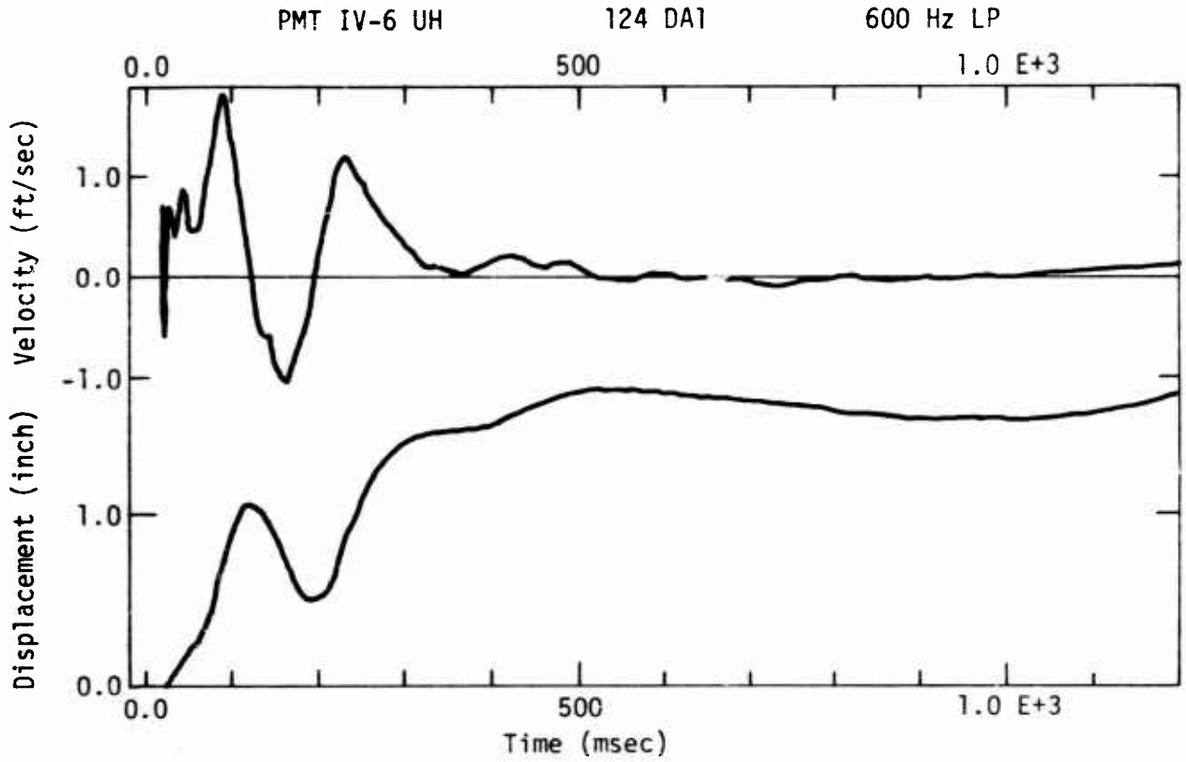

Figure 35. Horizontal Ground Motion, Station 5, Bell & Howell Accelerometer

APPENDIX

RESISTOR PARTS LIST

R Bal	20 kΩ	Potentiometer (Trimpot 224P-1-203)
R Cal	Precision 1 percent to be mounted on posts, value as per accelerometer	
R1	1 kΩ	1/2 Watt
R2	4.7 kΩ	1/2 Watt
R3	12 kΩ	1/2 Watt
R4	500 kΩ	Potentiometer 10 Turn
R5	500 kΩ	Potentiometer 10 Turn
R6	12 kΩ	1/2 Watt
R7	10 kΩ	1/2 Watt
R8	10 kΩ	1/2 Watt
R9	100 kΩ	1/2 Watt
R10	1 kΩ	Potentiometer (Bourns Trimpot 3059P-1-102)
R11	Selected Value	
R12	2.0 kΩ	1/2 Watt
R13	2.0 kΩ	1/2 Watt
R14	4.7 kΩ	1/2 Watt
R15	8.2 kΩ	1/2 Watt
R16	300 kΩ	1/2 Watt R1
R17	560 kΩ	1/2 Watt Rd
R18	1 megΩ	1/2 Watt R2
R19	1.5 megΩ	Potentiometer 10 Turn
R20	5 kΩ	1/2 Watt
R21	1 kΩ	1/2 Watt
R22	50 kΩ	1/2 Watt
R23	40 kΩ	1/2 Watt
R24	10 kΩ	1/2 Watt

CAPACITOR PARTS LIST

C1	0.01 µfd	Nonpolarized disk ceramic 15 WVDC
C2	0.01 µfd	Nonpolarized disk ceramic 15 WVDC
C3	1 µfd	Polarized electrolytic 15 WVDC

C4	0.1 µfd	Nonpolarized disk ceramic	15 WVDC
C5	0.01 µfd	Nonpolarized disk ceramic	15 WVDC
C6	1 µfd	Polarized electrolytic	15 WVDC
C7	0.01 µfd	Nonpolarized disk ceramic	15 WVDC
C8	0.01 µfd	Nonpolarized disk ceramic	15 WVDC
C9	10 µfd	Polarized electrolytic	25 WVDC
C10	0.002 µfd	Nonpolarized disk ceramic	25 WVDC
C11	0.002 µfd	Nonpolarized disk ceramic	25 WVDC
C12	2 µfd	Nonpolarized Tantalum	25 WVDC
C13	0.2 µfd	Nonpolarized Tantalum	25 WVDC
C14	0.02 µfd	Nonpolarized disk ceramic	25 WVDC
C15	5 µfd	Nonpolarized Tantalum	25 WVDC
C16	0.5 µfd	Nonpolarized Tantalum	25 WVDC
C17	0.05 µfd	Nonpolarized disk ceramic	25 WVDC
C18	10 µfd	Polarized electrolytic	50 WVDC
C19	10 µfd	Polarized electrolytic	50 WVDC
C20	10 µfd	Polarized electrolytic	50 WVDC
C21	1 µfd	Nonpolarized Tantalum	25 WVDC

SWITCH PARTS LIST

S1	Amp rocker	14 pin dip
S2	Amp rocker	14 pin dip
S3	Amp rocker	14 pin dip
S4	Amp rocker	14 pin dip
S5	Amp rocker	14 pin dip
S6	Amp rocker	14 pin dip
S7	Amp rocker	14 pin dip
S8	Amp rocker	8 pin dip
S9	Amp rocker	8 pin dip
S10	Amp rocker	8 pin dip
S11	Amp rocker	8 pin dip
S12	Grayhill right angle pushbutton	

RELAY PARTS

K1	Picareed PRME-1A00SC	14 pin dip
K2	Picareed PRME-1A00SC	14 pin dip

INTEGRATED CIRCUITS

U1	LM307	8 pin dip
U2	LM307	8 pin dip
U3	LM307	8 pin dip
U4	AD520J	14 pin dip
U5	NE555	8 pin dip
U6	NE555	8 pin dip

TRANSISTOR PARTS

Q1	2N718	TO18
Q2	2N718	TO18
Q3	2N718	TO18

DISTRIBUTION LIST

DEPARTMENT OF DEFENSE

Director
Defense Nuclear Agency
ATTN: PPSR
2 cy ATTN: STTI., Tech. Lib.
2 cy ATTN: SPSS

Director Defense Research and Engineering
ATTN: Asst. Dir. Strat. Wpns.

Director
Defense Intelligence Agency
ATTN: DI-7D
ATTN: DI-3

Director
Defense Advanced Research Projects Agency
ATTN: NMR

Commander
Field Command
Defense Nuclear Agency
ATTN: FCPR

Chief
Las Vegas Liaison Office
Field Command TD, DNA
ATTN: FCTC

Defense Documentation Center
2 cy ATTN: TC

Director
Joint Strategic Target Planning Staff
ATTN: JLTW

DEPARTMENT OF THE ARMY

Director
U.S. Army Ballistic Research Labs
ATTN: AMXBR-TB, J. Meszaros

Director
U.S. Army Waterways Exper. Sta.
ATTN: WESRL
ATTN: WESSS

DEPARTMENT OF THE NAVY

Commander
Naval Weapons Center
ATTN: Code 753

DEPARTMENT OF THE AIR FORCE

Headquarters
Air Force Systems Command
ATTN: DOB
ATTN: DLCAW

Commander-In-Chief
Strategic Air Command
ATTN: DEE

DEPARTMENT OF THE AIR FORCE (Continued)

HQ USAF/SA
ATTN: SAMI

AFTAC
ATTN: TAP

AFCEC
ATTN: PREC

AF Inspection and Safety Center
ATTN: PQAL

Commander
Air University Library
ATTN: LDE

Commander
Alaskan Air Command
ATTN: DEE

AF Institute of Technology
ATTN: Tech. Lib., Bldg. 640, Area B
ATTN: CES

U.S. Air Force Academy
ATTN: DFSLB

Air Force Systems Command Liaison Office
ATTN: Maj J. H. Pierson, Chief, LO

Commander
Rome Air Development Center
ATTN: Doc. Lib.
ATTN: DEE

AF Weapons Laboratory, AFSC
ATTN: HO
5 cy ATTN: SUL, Tech. Lib.
3 cy ATTN: DED

ENERGY RESEARCH & DEVELOPMENT ADMINISTRATION

Sandia Laboratories
ATTN: Org. 3141, Tech. Lib.

Sandia Laboratories
Livermore Laboratory
ATTN: Org. 8000, Tech. Info. Office

Division of Military Applications
U.S. Energy Rsch. & Dev. Admin.
ATTN: Dr. Rhodes

DEPARTMENT OF DEFENSE CONTRACTORS

Electromechanical Systems of New Mexico, Inc.
ATTN: Dr. R. A. Shunk

Physics International Company
ATTN: Mr. F. Saver

R & D Associates
ATTN: Dr. B. Hartenbaum

DEPARTMENT OF DEFENSE CONTRACTORS (Continued)

Stanford Research Institute
ATTN: Mr. D. Keough

Systems Science and Software
ATTN: Dr. D. Grine

DEPARTMENT OF DEFENSE CONTRACTORS (Continued)

Official Record Copy
ATTN: Capt Ray, DED